NASA
Technical
Paper
2726

August 1987

Experimental Evaluation of Heat Transfer on a 1030:1 Area Ratio Rocket Nozzle

Kenneth J. Kacynski,
Albert J. Pavli,
and Tamara A. Smith

NASA

NASA
Technical
Paper
2726

1987

Experimental Evaluation of Heat Transfer on a 1030:1 Area Ratio Rocket Nozzle

Kenneth J. Kacynski,
Albert J. Pavli,
and Tamara A. Smith

Lewis Research Center
Cleveland, Ohio

National Aeronautics
and Space Administration

**Scientific and Technical
Information Office**

Summary

Accurate determination of heat flux in the divergent portion of high-area-ratio rocket nozzles is important not only in designing the nozzles but also in predicting their performance. Although much work has been done in obtaining experimental heat-flux values in the chamber and throat sections of rocket engines, little data has been taken in the divergent portion, especially for high-area-ratio nozzles (200:1 to 1000:1).

At the NASA Lewis Research Center Rocket Engine Test Facility, a 1030:1 carbon steel, heat-sink nozzle was tested. The test conditions included a nominal chamber pressure of 2413 kN/m^2 (350 psia) and a mixture ratio range of 2.78 to 5.49. The propellants used were gaseous oxygen and gaseous hydrogen. The nozzle had thermocouples placed on the outer wall at various axial locations. The outer-wall temperature measurements were used to calculate the inner-wall temperature and the heat flux and heat rate to the nozzle at specified axial locations.

The experimental heat fluxes were compared to those predicted by the December 1984 version of the Two-Dimensional Kinetics (TDK) computer analysis program. When laminar boundary-layer flow was assumed in the analysis, the predicted values were within 15 percent of the experimental values for area ratios of 20 to 975. However, when turbulent boundary-layer conditions were assumed, the predicted values were approximately 120 percent higher than the experimental values. A study was performed to determine if the conditions within the nozzle could sustain a laminar boundary layer. Using the flow properties predicted by TDK, we calculated the momentum-thickness Reynolds number and predicted the point of transition to turbulent flow. The predicted transition point was within 0.5 in. of the nozzle throat. Calculations of the acceleration parameter were then made to determine if the flow conditions could produce relaminarization of the boundary layer. It was determined that if the boundary-layer flow was inclined to transition to turbulent, the acceleration conditions within the nozzle would tend to suppress turbulence and keep the flow laminarlike.

Introduction

The design of future rocket engines for space application requires the optimization of many parameters to achieve the most effective configuration. Because of the tradeoffs that must be made between components and systems, predictions must be made of both the performance of these components and the effect of changes in these components on the overall performance of the engine. Because of the large physical size of high-area-ratio nozzles, decisions regarding exact primary nozzle size, size of extensions, and materials needed to achieve desired performance tradeoffs can sometimes become clouded. The predictions of nozzle performance, especially at high expansion area ratios, do not have the accuracy needed. One ingredient necessary for an accurate modeling of nozzle performance is an accurate representation of the heat transfer to the wall of the nozzles. Knowledge of the heat transfer is also important in determining the amount and type of cooling necessary and in selecting materials for the wall of the nozzle. Hence, an experimental program was conducted to obtain some of these data. The tests were performed in the altitude test chamber at the NASA Lewis Research Center Rocket Engine Test Facility.

In this report, heat-transfer results are presented from test data obtained for a 1030:1 carbon steel nozzle. This nozzle was a heat-sink configuration and had thermocouples placed on the outer surface at several axial locations. The nozzle was test-fired using gaseous hydrogen and gaseous oxygen as propellants. The chamber pressure was nominally 2413 kN/m^2 (350 psia), the propellant mixture ratio O/F range was 2.78 to 5.49, and the firing duration was 3 sec. From the measured outer-wall temperature data, inner-wall temperatures and heat fluxes were calculated. From these results, the heat rate to the nozzle wall at specific axial locations was determined. These experimental heat-transfer results were then compared to the values predicted by the December 1984 version of the TDK computer program (ref. 1).

Symbols

A	area, m^2
A_s	nozzle surface area
C_v	specific heat at constant volume, J/kg K
D	diameter, m
$I_{sp,V}$	vacuum specific impulse
K	acceleration parameter
K_{ax}	axisymmetric acceleration parameter
k	conductivity, W/m K

L	axial length, m
O/F	propellant mixture ratio
$P_{c,e}$	effective chamber pressure, kN/m^2
Q	heat rate, W
q''	heat flux, W/m^2
R	local radius, m
Re_θ	momentum-thickness Reynolds number
r	radius, m
T	temperature, K
t	time, sec
u	velocity, m/sec
x	axial distance from throat, m
α	diffusivity, m^2/sec
γ	ratio of specific heats
ϵ	nozzle expansion area ratio
η_{C^*}	characteristic exhaust velocity efficiency, percent
θ	angle between nozzle wall and axis, deg
μ	viscosity, N-sec/m^2
ν	kinematic viscosity, m^2/sec
ρ	density, kg/m^3

Subscripts:

a	ambient
c	ceramic coating
e	boundary-layer edge conditions
i	inner wall
n	nickel
o	outer wall
s	surface
z	interface
∞	freestream

Apparatus

Test Facility

Testing was done in the new altitude test capsule at the NASA Lewis Rocket Engine Test Facility (RETF). Figure 1(a) shows cutaway views of the test capsule and spray cooler, and figure 1(b) is a schematic diagram of the facility. The water-jacketed second throat diffuser connects the test capsule to the spray cooler. The kinetic energy of the rocket exhaust gases was used in this diffuser to accomplish some of the altitude pumping of the test capsule. The facility was able to provide test-capsule pressures of 206.8 to 344.7 N/m^2 (0.03 to 0.05 psia) while exhausting the gas into the spray cooler at pressures of 2068.4 to 4136.9 N/m^2 (0.3 to 0.6 psia). The exhaust gases were removed from the spray cooler by two means. Approximately half of the exhaust gases (product of hydrogen/oxygen combustion) were condensed to water in the spray cooler. This water, along with the cooling spray water, exited the spray cooler through a vertical drain line into the cylindrical detention tank. This vertical drain line functioned as a barometric leg, allowing water to exit while preventing atmospheric air from entering the spray cooler. The remaining exhaust gases (the noncondensibles) were pumped by the gaseous-nitrogen-driven ejectors shown mounted on top of the spray cooler. Four ejectors, connected in a series-parallel arrangement, provided two trains of two stages each. The exhaust from these ejectors was directed up through two short stacks and vented to the atmosphere.

The test capsule was constructed in two parts. One part was the fixed end onto which the research hardware was mounted. The other part was the movable can, which could be rolled back to provide access to the experiment. The inside of the test capsule can be seen in figure 2. This photograph shows the horizontal thrust stand with a test nozzle and a combustor installed on the fixed end and the rest of the test capsule rolled back. The nozzle shown is the 1030:1 nozzle. Mounted above the nozzle are the pressure transducers used to measure nozzle static pressure. Visible alongside the nozzle are some of the wall-temperature thermocouples in the process of being connected.

The thrust stand could measure 13.34 kN (3000 lb) of thrust full scale and was attached to a foundation that was separate from the test capsule bulkhead. The thrust structure passed through the test capsule bulk head by means of isolation ports that were sealed by metal bellows and was attached to the concrete outside the test capsule. The thrust stand was designed to have a 2σ variation of less than ± 0.1 percent of full-scale thrust. While at altitude the thrust stand could be calibrated remotely against an additional load cell. This calibration load cell had a 2σ variation of less than ± 0.05 percent of full scale and a calibration traceable to the National Bureau of Standards.

Test Hardware

The carbon steel nozzle that was tested had a 2.54-cm-(1-in.-) diameter throat and expanded to an area ratio of 1030. It was designed by the following procedure. Initially, the Rao nozzle contour program (ref. 2) was run specifying certain properties including a ratio of specific heats γ of 1.23, a throat radius of 1.27 cm (0.5 in.), a chamber pressure of 6895 kN/m^2 (1000 psia), an area ratio of 1000, and a nozzle length equivalent to 100 percent of a 15° cone. The Rao program uses the method of characteristics to calculate an optimum contour for an ideal-gas, constant-γ expansion. Conditions within the Rao contour were predicted using a one-dimensional kinetics analysis program (ref. 3). The input conditions to the kinetics program included a chamber pressure of 6895 kN/m^2 (1000 psia), a mixture ratio of 6, a throat radius of 1.27 cm (0.5 in.), and hydrogen/oxygen combustion reactions. The

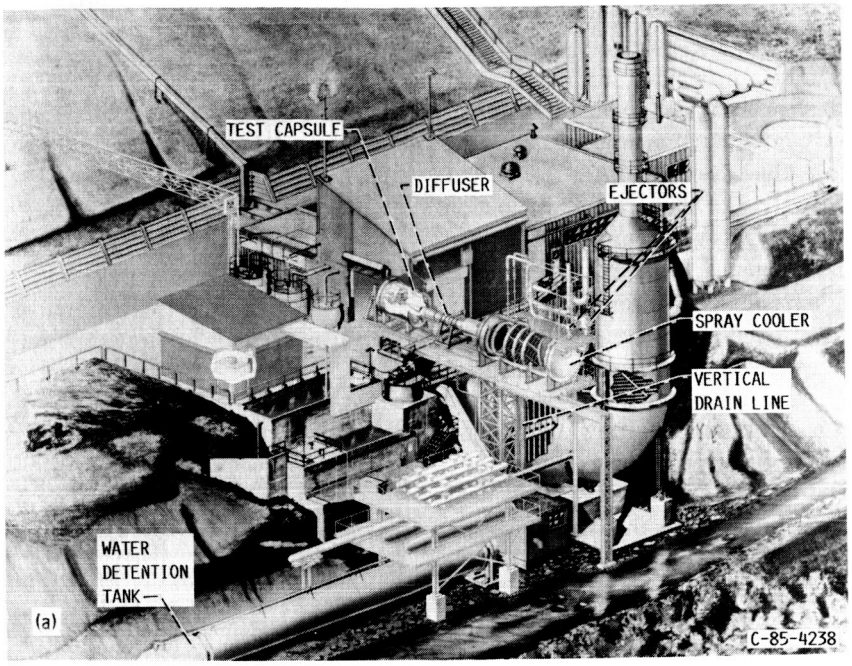

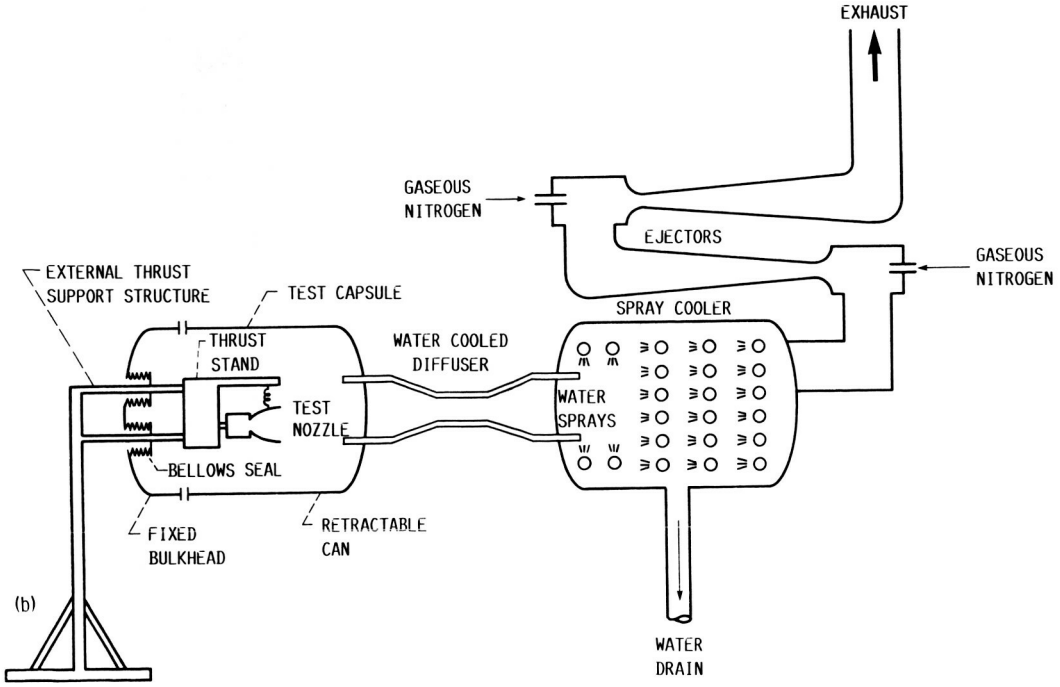

(a) Cutaway view of altitude test capsule and spray cooler.
(b) Schematic of altitude test facility.
Figure 1.—NASA Lewis Research Center Rocket Engine Test Facility (RETF).

one-dimensional kinetics program developed at NASA Lewis uses an implicit finite-difference technique to integrate the differential equations of chemical kinetics. Output from the kinetics program was used with the Boundary-Layer Integral Matrix Procedure (BLIMP–J) computer program (ref. 4) to determine the characteristics of the boundary layer. The BLIMP–J computer program can compute the nonsimilar, chemically reacting laminar or turbulent boundary layer for nonablating internal flow configurations. In addition to the properties calculated in the kinetics program for the 1000:1 nozzle, an estimated inner-wall axial temperature distribution was input to BLIMP–J. Other inputs to this program included the Cebeci-Smith turbulence model, the Buddenber-Wilke mixture formula for viscosity, and the Maxon-Saxena model with a Eucken correction for thermal conductivity. The program estimates the boundary-layer displacement thickness along the nozzle length. This displacement thickness was added to the Rao contour at all stations along the flow axis. Thus, a new contour was produced that had an estimated "inviscid" core in the center with the boundary-layer displacement thickness added to the outside. This was the contour of the test nozzle and is shown in figure 3.

The nozzle was fabricated in three parts. The first part consisted of the convergent section, the throat, and the divergent section that expanded to an area ratio of 29.9:1. It was made of 0.635-cm- (0.25-in.-) thick electroformed nickel with an alumina ceramic coating approximately 0.01016-cm (0.004-in.) thick on the inside surface. The second part was an expansion skirt that went from the 29.9:1 to the 427.5:1 expansion area ratio. It was made of 0.635-cm- (0.25-in.-) thick carbon steel. The third part was a continuation of the expansion skirt from an area ratio of 427.5 to an area ratio of 1030. It was also made of 0.635-cm (0.25-in.) carbon steel.

The combustor used in this program was uncooled and relied on its thermal inertia to survive the short firings (<3 sec). Gaseous hydrogen and gaseous oxygen were supplied at ambient temperatures from high-pressure storage bottles and were used as propellants for the combustor. The injector was a gaseous oxygen shower head with gaseous hydrogen flowing through the porous face plate. It had 36 gaseous oxygen streams arranged in a circular pattern. The igniter torch assembly, which also used gaseous hydrogen and gaseous oxygen as propellants, employed a spark plug as an ignition source and was located in the center of the injector.

Instrumentation

Outer-wall temperatures were measured by chromel-constantan thermocouples spot-welded to the nozzle surface. These thermocouples were referenced to a 340 K (150 °F) oven. Their specified absolute accuracy was ±1.1 K (±2 °F). The locations of the thermocouples corresponded to the area ratios 5.6, 12, 20, 50, 100, 200, 300, 388, 500, 635, 800, and 975.

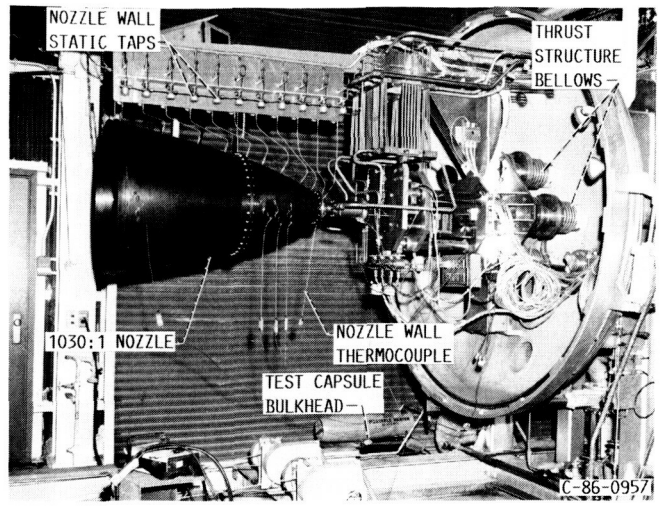

Figure 2.—Inside of altitude test capsule.

NOZZLE COORDINATES

AXIAL DISTANCE FROM THROAT		RADIUS	
cm	in.	cm	in.
0.0000	0.0000	1.2700	0.5000
.3929	.1547	1.4371	.5658
.4641	.1827	1.4961	.5890
.6068	.2389	1.6190	.6374
.7503	.2954	1.7404	.6852
.8230	.3240	1.8031	.7099
1.3246	.5215	2.2426	.8829
1.7844	.7025	2.6515	1.0438
2.3777	.9361	3.1643	1.2458
3.2062	1.2623	4.2001	1.6536
7.0256	2.7660	6.6703	2.6261
7.8931	3.1075	7.2426	2.8514
9.6269	3.7901	8.3320	3.2803
10.6505	4.1931	8.9433	3.5210
11.6738	4.5960	9.5341	3.7536
12.9022	5.0796	10.2189	4.0232
15.3429	6.0405	11.5108	4.5318
16.5392	6.5115	12.1150	4.7697
19.5651	7.7028	13.5702	5.3426
23.3688	9.2003	15.2710	6.0122
25.4869	10.0342	16.1651	6.3642
29.5410	11.6303	17.7871	7.0028
33.7297	13.2794	19.3558	7.6204
36.2996	14.2912	20.2705	7.9805
38.8696	15.3030	21.1524	8.3277
41.4193	16.3068	21.9977	8.6605
47.2194	18.5903	23.8201	9.3780
51.1703	20.1458	24.9895	9.8384
55.1213	21.7013	26.1064	10.2781
60.4944	23.8167	27.5486	10.8459
71.1091	27.9957	30.1694	11.8777
76.2211	30.0083	31.3365	12.3372
90.6396	35.6849	34.3444	13.5214
105.0371	41.3532	36.9933	14.5643
113.0838	44.5212	38.3365	15.0931
128.5725	50.6191	40.6598	16.0078

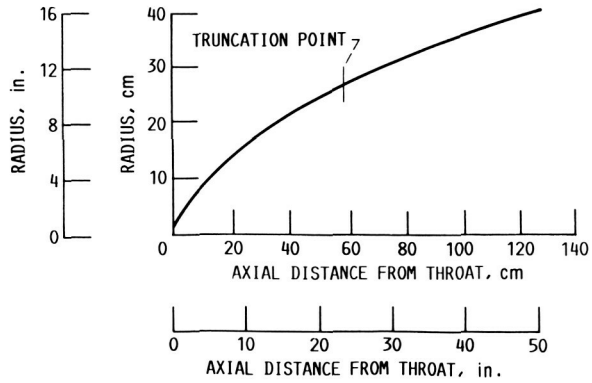

Figure 3.—Nozzle contour and coordinates.

Propellant flow rates were measured by calibrated venturis. The vacuum reference pressure was measured by a thermocouple vacuum gauge, and the rest of the pressures were measured by strain-gauge-bridge pressure transducers. These transducers were of two types: absolute pressure transducers and differential pressure transducers. The very low pressures from the static pressure taps on the nozzle wall and the test-capsule altitude pressure were measured by the differential pressure transducers. These units were then referenced to the vacuum reference pressure tank through a network of automatic shutoff and bypass valves. These transducers had only low ranges of differential pressure, 4.1 and 34.0 kN/m^2 (0.60 and 5.0 psi) full scale and could not tolerate a differential pressure of 1 atm across their diaphragms.

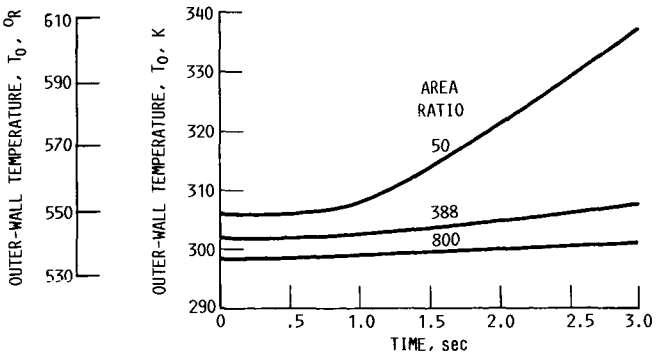

Figure 4.—Measured outer-wall temperature time history for three thermocouple locations (reading 121).

Methods and Procedure

Experimental Heat Flux

During the performance testing of the 1030:1 nozzle, the nozzle outer-wall temperatures were measured at several axial locations. These thermocouple measurements were taken at a rate of 50/sec, averaged in groups of five, and displayed at 0.1-sec intervals. Table I displays the thermocouple measurements taken immediately before the engine was shut down. At this point in the testing, the engine was at steady state with regard to the static pressure measurements in the nozzle. The following discussion describes the procedure that was used to determine inner-wall temperature and heat flux from the thermocouple measurements in table I.

The heat flux and the inner-wall temperature at each thermocouple location can be determined by solving the following differential equation:

$$\rho C_v\left(\frac{\partial T}{\partial t}\right) = \frac{1}{r}\frac{\partial}{\partial r}\left[(kr)\frac{\partial T}{\partial r}\right] \tag{1}$$

A detailed solution is shown in appendix A. In deriving equation (1), we assumed that axial conduction along the nozzle wall and heat transfer from the outer wall were negligible. An order-of-magnitude analysis of these two assumptions is presented in appendix B. An assumption of constant properties was also made.

TABLE I.—EXPERIMENTALLY MEASURED NOZZLE TEMPERATURES

Reading	Effective chamber pressure, $P_{c,e}$, kN/m^2 (psia)	Propellant mixture ratio, O/F	Characteristic exhaust velocity, C^*, m/sec (ft/sec)	Characteristic exhaust velocity efficiency, η_{C^*}, percent	Expansion area ratio, ϵ											
					5.6	12	20	50	100	200	300	388	500	635	800	975
					Measured nozzle wall temperature on outside diameter surface, K (°R)											
112	2482 (360.0)	3.84	2402 (7880)	95.5	341.05 (613.89)	349.25 (628.65)	333.91 (601.03)	319.49 (575.08)	306.65 (551.97)	299.70 (539.46)	289.98 (521.97)	296.06 (532.90)	286.65 (515.97)	292.78 (527.00)	285.53 (513.95)	290.87 (523.56)
113	2461 (356.9)	4.36	2346 (7697)	95.0	352.08 (633.15)	361.34 (650.42)	348.13 (626.64)	336.09 (604.97)	322.42 (580.35)	312.87 (563.17)	302.25 (544.05)	305.08 (549.14)	295.23 (531.42)	298.86 (537.94)	292.08 (525.75)	295.16 (531.28)
114	2488 (360.9)	5.08	2283 (7491)	94.4	366.21 (659.18)	369.33 (664.80)	357.51 (643.51)	346.14 (623.06)	331.17 (596.11)	320.81 (577.45)	310.71 (559.28)	311.89 (561.41)	302.02 (543.64)	303.22 (545.80)	296.21 (533.18)	297.39 (535.30)
115	2450 (355.3)	5.49	2244 (7363)	94.2	364.98 (656.96)	369.68 (665.43)	361.88 (651.39)	356.28 (641.30)	341.84 (615.32)	329.66 (593.38)	318.62 (573.52)	318.25 (572.85)	307.76 (553.97)	307.53 (553.56)	200.03 (540.06)	299.91 (539.83)
117	2456 (356.2)	3.19	2453 (8048)	96.4	333.27 (599.89)	346.29 (623.32)	348.13 (626.64)	353.61 (636.49)	345.83 (622.50)	336.60 (605.88)	326.88 (588.39)	325.63 (586.13)	315.68 (568.22)	314.68 (566.42)	308.32 (554.97)	307.76 (553.97)
120	2449 (355.2)	4.30	2377 (7799)	95.7	369.94 (665.89)	346.89 (624.40)	336.89 (606.41)	335.05 (603.09)	349.38 (528.89)	314.71 (566.47)	310.43 (558.78)	307.28 (553.10)	303.98 (547.17)	304.16 (547.49)	300.90 (541.62)	298.16 (536.69)
121	2482 (306.0)	4.11	2418 (7934)	96.8	357.53 (643.56)	348.94 (628.10)	345.07 (621.12)	337.31 (607.15)	321.92 (579.46)	312.34 (562.22)	309.30 (556.74)	307.11 (552.79)	304.47 (548.04)	301.49 (542.68)	300.39 (540.70)	297.38 (536.09)
123	2449 (355.2)	3.19	2508 (8228)	98.4	327.76 (598.97)	333.86 (600.94)	328.58 (591.44)	322.02 (579.64)	311.89 (561.41)	306.85 (552.33)	305.71 (550.28)	309.24 (547.63)	302.61 (544.70)	300.13 (540.24)	299.78 (539.60)	297.52 (535.54)
124	2492 (361.4)	2.78	2543 (8342)	99.4	328.31 (590.95)	335.14 (603.26)	331.73 (597.12)	332.34 (598.22)	323.23 (581.82)	316.95 (570.51)	313.80 (564.84)	310.84 (559.51)	307.84 (554.11)	305.05 (549.09)	304.26 (547.67)	302.05 (543.69)
125	2441 (354.0)	3.74	2451 (8042)	97.2	347.34 (625.22)	342.74 (616.93)	340.52 (612.94)	344.95 (620.91)	334.90 (602.82)	326.32 (587.37)	321.72 (579.10)	317.92 (572.26)	313.78 (564.80)	310.28 (558.51)	308.92 (556.06)	305.81 (550.46)

Equation (1) was solved by further assuming that the temperature rise with respect to time $\partial T/\partial t$ is independent of time (quasi-steady-state). It was also assumed that $\partial T/\partial t$ is constant for both materials (nickel and ceramic) in a two-material system. Representative temperature responses from experimental reading 121 are presented in figure 4. This figure shows that the quasi-steady-state assumption is applicable for time greater than approximately 1 sec. Therefore, the values for $\partial T/\partial t$ that were used to determine inner-wall temperature and heat flux were taken from the last second of firing and were averaged over this 1-sec time period. These values are presented in table II.

Using the assumptions mentioned previously reduces above the differential energy equation to the following for a two-material system (ceramic coating on a nickel wall):

$$T_i = T_o + \frac{(\partial T/\partial t)}{4\alpha_c}\left(R_i^2 - R_z^2\right) + \left\{\frac{(\partial T/\partial t)}{4\alpha_n}\left[R_z^2 - R_o^2 - R_o^2 \ln\left(\frac{R_z}{R_o}\right)^2\right]\right\} + \frac{(\partial T/\partial t)k_n}{2\alpha_n k_c}\left(\ln\frac{R_i}{R_z}\right)\left(R_z^2 - R_o^2 - R_z^2\frac{\alpha_n k_c}{\alpha_c k_n}\right) \quad (2)$$

and

$$q_i'' = \frac{(\partial T/\partial t)k_n}{2R_i\alpha_n}\left(R_o^2 - R_z^2\right) + \frac{(\partial T/\partial t)k_c}{2\alpha_c R_i}\left(R_z^2 - R_i^2\right) \quad (3)$$

For a single-material system (carbon steel wall), the solution simplifies to

$$T_i = T_o - \frac{R_o^2}{4\alpha}\frac{\partial T}{\partial t}\left[1 - \left(\frac{R_i}{R_o}\right)^2 + \ln\left(\frac{R_i}{R_o}\right)^2\right]$$

$$q_i'' = \frac{kR_i}{2\alpha}\frac{\partial T}{\partial t}\left[\left(\frac{R_o}{R_i}\right)^2 - 1\right] \quad (4)$$

The inner-wall temperature and the heat flux can be determined by using equations (2) to (4) and the experimental measurements of the outer-wall temperature T_o and its time history $\partial T/\partial t$.

Heat Rate

The heat rate Q to the walls of a rocket nozzle between two axial locations can be determined by integrating the heat-flux values with respect to nozzle surface area:

TABLE II.—EXPERIMENTALLY MEASURED RATES OF INCREASE IN NOZZLE TEMPERATURE

Reading	Effective chamber pressure, $P_{c,e}$, kN/m² (psia)	Propellant mixture ratio, O/F	Characteristic exhaust velocity, C^*, m/sec (ft/sec)	Characteristic exhaust velocity efficiency, η_{C^*}, percent	Expansion area ratio, ϵ											
					5.6	12	20	50	100	200	300	388	500	635	800	975
					Measured rate of increase in nozzle temperature, K/sec (°R)											
112	2482 (360.0)	3.84	2402 (7880)	95.5	35.14 (63.26)	37.36 (67.25)	26.22 (47.19)	16.94 (30.50)	9.27 (16.69)	4.85 (8.73)	3.31 (5.95)	2.66 (4.78)	2.03 (3.66)	1.53 (2.75)	1.21 (2.17)	1.01 (1.82)
113	2461 (356.9)	4.36	2346 (7697)	95.0	38.11 (68.59)	39.09 (70.36)	28.33 (50.99)	17.77 (31.99)	9.81 (17.65)	5.31 (9.56)	3.63 (6.53)	2.94 (5.30)	2.24 (4.04)	1.69 (3.04)	1.35 (2.43)	1.06 (1.90)
114	2488 (360.9)	5.08	2283 (7491)	94.4	45.44 (81.80)	41.27 (74.28)	30.27 (54.49)	19.58 (35.25)	10.89 (19.61)	5.80 (10.44)	3.91 (7.04)	3.20 (5.76)	2.51 (4.51)	1.89 (3.40)	1.36 (2.45)	1.06 (1.90)
115	2450 (355.3)	5.49	2244 (7363)	94.2	44.46 (80.03)	41.14 (74.06)	30.76 (55.36)	19.63 (35.33)	10.91 (19.63)	5.77 (10.39)	3.96 (7.13)	3.37 (6.06)	2.51 (4.51)	2.03 (3.65)	1.36 (2.44)	1.07 (1.93)
117	2456 (356.2)	3.19	2453 (8048)	96.4	25.67 (46.20)	27.04 (48.67)	20.31 (36.55)	11.93 (21.48)	6.44 (11.60)	3.57 (6.43)	2.47 (4.44)	2.14 (3.86)	1.65 (2.97)	1.26 (2.26)	.96 (1.73)	.89 (1.60)
120	2449 (355.2)	4.30	2377 (7799)	95.7	43.04 (77.48)	30.36 (54.64)	23.68 (42.63)	15.67 (28.21)	9.61 (17.30)	5.30 (9.54)	3.51 (6.31)	2.99 (5.38)	2.19 (3.94)	1.58 (2.85)	1.15 (2.07)	.87 (1.57)
121	2482 (306.0)	4.11	2418 (7934)	96.8	36.86 (66.35)	26.77 (48.19)	23.24 (41.84)	16.41 (29.54)	9.43 (16.98)	4.96 (8.93)	3.33 (6.00)	2.79 (5.02)	2.09 (3.76)	1.53 (2.76)	1.07 (1.93)	.84 (1.52)
123	2449 (355.2)	3.19	2508 (8228)	98.4	26.09 (46.97)	24.82 (44.68)	22.94 (41.30)	13.73 (24.71)	7.37 (13.27)	3.91 (7.03)	2.56 (4.61)	2.27 (4.08)	1.63 (2.94)	1.20 (2.16)	.87 (1.57)	.69 (1.24)
124	2492 (361.4)	2.78	2543 (8342)	99.4	22.07 (39.73)	22.55 (40.59)	20.51 (36.91)	12.43 (22.38)	6.45 (11.61)	3.55 (6.39)	2.33 (4.20)	2.09 (3.77)	1.44 (2.60)	1.07 (1.92)	.82 (1.47)	.77 (1.38)
125	2441 (354.0)	3.74	2451 (8042)	97.2	32.25 (58.05)	24.41 (43.93)	21.81 (39.26)	15.02 (27.03)	8.33 (15.00)	4.34 (7.82)	2.93 (5.27)	2.54 (4.58)	1.88 (3.39)	1.33 (2.40)	.96 (1.72)	.81 (1.46)

$$Q = \int_{L_1}^{L_2} q'' \, dA_s \tag{5}$$

Furthermore, the differential surface area can be written

$$dA_s = \frac{\pi D_i dL}{\cos \theta} \tag{6}$$

and, thus, the heat rate is

$$Q = \int_{L_1}^{L_s} \left(\frac{q'' \pi D_i}{\cos \theta} \right) dL \tag{7}$$

Analysis

Experimental results were compared with analytical predictions. The following section contains a description of the analytical computer program and the procedure with which it was used.

The TDK computer program evaluates the two-dimensional and viscous effects on the performance of rocket exhaust nozzles (ref. 1). The version of TDK used in this report was version 2.4, December 1984. TDK consists of a one-dimensional equilibrium analysis, a one-dimensional kinetic analysis, a two-dimensional kinetic analysis, and a boundary-layer analysis. The boundary-layer module (BLM) of the TDK program calculates compressible laminar and turbulent wall boundary layers in axisymmetric nozzles. BLM uses the two-point finite-difference method developed by Keller and Cebeci (ref. 5) to calculate the boundary-layer properties and the Cebeci-Smith eddy-viscosity formulation (ref. 6) to model the turbulent boundary layer.

The hardware specifications and experimental test conditions were used to write the input files to TDK so that this program could accurately model the nozzle performance. The input variables that described the nozzle inlet geometry are listed in table III. The nozzle contour coordinates that were used are shown in figure 3. Table IV shows experimental values that were also used in the TDK input files: effective chamber pressure, propellant mixture ratio, fuel injection temperature, and oxidizer injection temperature. Each analytical result corresponds to an experimental reading. The experimentally determined inner-wall temperatures, which are listed in table V, were also used in the input files.

Conditions within the combustion chamber and convergent nozzle had to be estimated because no experimental data was available. When inner-wall temperatures for the chamber and convergent section were calculated, transient radial heat conduction and a run time of three seconds were assumed. The temperature, pressure, and velocity distributions of the flow within the combustion chamber (which were used in the boundary-layer analysis) were estimated using one-dimensional equilibrium predictions.

TDK was run initially with the default value for transition to turbulence. This default value made the transition to turbulent flow occur within the combustion chamber. The results from those initial runs indicated that the predicted heat fluxes within the divergent nozzle were significantly higher than the experimentally determined heat fluxes. Also, the overall predicted performance was significantly lower than the measured performance (ref. 7). Therefore, the analysis was performed again with the location of transition set beyond the exit plane of the nozzle (completely laminar flow).

Appendix C contains the input files to TDK which correspond to experimental readings 112 to 115, 120, and 121. Only these experimental readings could be modeled because the TDK program could not run to completion for mixture ratios below 3.84. This version of the TDK program was originally written for much lower area ratio rocket nozzle conditions. The inability of the program to run below an O/F of 3.84 is due to the low-pressure/low-temperature conditions, which are predicted as the flow expands to an area ratio of 1030.

TABLE III.—TWO-DIMENSIONAL KINETICS (TDK) INPUT VARIABLES

Parameter	TDK variable	Value
Throat radius, cm (in.)	RSI	1.27(0.5)
Inlet contraction ratio	ECRAT	4.223
Inlet wall radius[a]	RI	2.0
Inlet angle, deg	THETAI	25.0
Upstream wall radius of curvature[a]	RWTU	2.0
Downstream wall radius of curvature[a]	RWTD	0.4
Nozzle attachment angle, deg	THETA	39.41
Nozzle exit angle, deg	THE	[b]7.94

[a]Normalized by throat radius.
[b]THE = 15.5 for truncated contour.

Results and Discussion

Experimental Results

Investigating heat transfer in high-area-ratio nozzles is part of an overall high-area-ratio rocket engine performance program. Results from the performance testing (ref. 8) are presented in table IV. The following is a discussion of the heat-transfer results obtained using the experimentally measured outer-wall temperatures. These results are presented in tables V and VI. Table V contains the calculated nozzle inner-wall temperatures, and table VI contains the calculated heat flux to the nozzle wall.

TABLE IV.—EXPERIMENTAL RESULTS

[Nozzle exit expansion area ratio, ϵ, 1030.]

Reading	Effective chamber pressure $P_{c,e}$, kN/m^2 (psia)	Propellant mixture ratio, O/F	Fuel injection pressure, kN/m^2 (psia)	Fuel injection temperature, K (°R)	Oxidizer injection pressure, kN/m^2 (psia)	Oxidizer injection temperature, K (°R)	Propellant flow rate, kg/sec (lb/sec)	Vacuum thrust, F_v, N (lb)
112	2482 (360.0)	3.84	3061 (444.0)	285.6 (514.1)	2809 (407.4)	279.2 (502.5)	0.5266 (1.161)	2422 (544.4)
113	2461 (356.9)	4.36	2956 (428.8)	284.2 (511.5)	2818 (408.7)	277.0 (498.6)	.5334 (1.176)	2409 (541.6)
114	2488 (360.9)	5.08	2912 (422.4)	283.9 (511.1)	2890 (419.2)	275.8 (496.4)	.5543 (1.222)	2457 (552.3)
115	2450 (355.3)	5.49	2843 (412.4)	283.5 (510.3)	2870 (416.3)	275.9 (496.6)	.5552 (1.224)	2448 (550.4)
117	2456 (356.2)	3.19	3160 (458.3)	281.1 (506.0)	2735 (396.7)	275.1 (495.2)	.5094 (1.123)	2364 (531.5)
120	2449 (355.2)	4.30	2950 (427.8)	294.4 (529.9)	2803 (406.6)	287.5 (517.5)	.5316 (1.172)	2429 (546.1)
121	2482 (360.0)	4.11	3013 (437.0)	295.0 (531.0)	2832 (410.7)	288.3 (518.9)	.5293 (1.167)	2459 (552.9)
123	2449 (355.2)	3.19	3152 (457.2)	295.6 (532.0)	2732 (396.2)	289.4 (521.0)	.5039 (1.111)	2377 (534.3)
124	2492 (361.4)	2.78	3328 (482.7)	295.9 (532.6)	2752 (399.1)	289.5 (521.1)	.5058 (1.115)	2386 (536.4)
125	2441 (354.0)	3.74	3028 (439.1)	296.3 (533.3)	2763 (400.7)	289.2 (520.6)	.5135 (1.132)	2406 (541.0)

Reading	Ambient pressure around the nozzle, P_a, kN/m^2 (psia)	Characteristic exhaust velocity C^*, m/sec (ft/sec)	Characteristic exhaust velocity efficiency, η_{C^*}, percent	Measured vaccum thrust coefficient, $C_{F,V}$	Thrust coefficient efficiency, $\eta_{C_{F,V}}$, percent	Vacuum specific impulse, $I_{sp,V}$, sec	Vacuum specific impulse efficiency, $\eta I_{sp,V}$, percent
112	0.2682 (0.0389)	2402 (7880)	95.5	1.917	97.3	468.9	92.9
113	.2592 (.0376)	2346 (7697)	95.0	1.914	95.3	460.4	90.5
114	.2530 (.0367)	2283 (7491)	94.4	1.941	94.0	451.9	88.8
115	.2530 (.0367)	2244 (7363)	94.2	1.967	93.7	449.7	88.3
117	.2461 (.0357)	2453 (8048)	96.4	1.892	98.4	473.4	94.9
120	.2544 (.0369)	2377 (7799)	95.7	1.923	96.0	466.1	91.8
121	.2654 (.0385)	2418 (7934)	96.8	1.921	96.6	473.6	93.5
123	.2592 (.0376)	2508 (8228)	98.4	1.881	97.7	481.1	96.2
124	.2441 (.0354)	2543 (8342)	99.4	1.857	97.8	481.3	97.3
125	.2420 (.0351)	2451 (8042)	97.2	1.912	97.4	477.8	94.6

TABLE V.—EXPERIMENTALLY DETERMINED NOZZLE TEMPERATURES

Reading	Effective chamber pressure, $P_{c,e}$, kN/m^2 (psia)	Propellant mixture ratio, O/F	Characteristic exhaust velocity, C^*, m/sec (ft/sec)	Characteristic exhaust velocity efficiency, η_{C^*}, percent	Expansion area ratio, ϵ											
					5.6	12	20	50	100	200	300	388	500	635	800	975
					Calculated nozzle inside wall temperature on inner diameter surface K (°R)											
112	2482 (360.0)	3.84	2402 (7880)	95.5	560.34 (1008.61)	577.36 (1039.24)	492.25 (886.05)	339.06 (610.30)	317.30 (571.14)	302.25 (549.45)	293.76 (528.76)	299.08 (538.35)	288.99 (520.14)	294.51 (530.12)	286.90 (516.42)	292.01 (525.62)
113	2461 (356.9)	4.36	2346 (7697)	95.0	589.85 (1061.73)	600.00 (1080.00)	519.23 (934.61)	356.62 (641.91)	333.68 (600.62)	318.95 (574.11)	306.39 (551.50)	308.43 (555.18)	298.13 (536.63)	300.78 (541.40)	293.62 (528.52)	296.36 (533.44)
114	2488 (360.9)	5.08	2283 (7491)	94.4	649.77 (1169.58)	626.84 (1128.31)	540.34 (972.62)	368.76 (663.76)	343.69 (618.64)	327.44 (589.39)	315.17 (567.31)	316.66 (569.98)	304.88 (548.78)	305.37 (549.66)	297.76 (535.97)	298.59 (537.46)
115	2450 (355.3)	5.49	2244 (7363)	94.2	642.40 (1156.32)	620.89 (1117.60)	547.64 (985.76)	378.94 (682.10)	354.37 (637.87)	335.14 (603.26)	323.14 (581.66)	322.09 (579.76)	310.62 (559.11)	309.84 (557.71)	301.58 (542.84)	301.12 (542.02)
117	2456 (356.2)	3.19	2453 (8048)	96.4	493.42 (888.16)	511.37 (920.47)	470.78 (847.40)	367.38 (661.29)	353.24 (635.83)	340.68 (613.23)	329.70 (593.46)	328.07 (590.53)	317.59 (571.67)	316.11 (568.99)	309.41 (556.94)	308.77 (555.79)
120	2449 (355.2)	4.30	2377 (7799)	95.7	638.52 (1149.34)	532.22 (958.00)	479.91 (863.83)	353.14 (635.66)	304.87 (548.76)	320.77 (577.38)	314.43 (565.98)	310.68 (559.23)	306.48 (551.66)	305.96 (550.73)	302.21 (543.98)	299.15 (538.47)
121	2482 (360.0)	4.11	2418 (7934)	96.8	587.53 (1057.56)	512.40 (922.32)	485.46 (873.83)	356.26 (641.26)	332.76 (598.97)	318.02 (572.43)	313.11 (563.59)	310.28 (558.51)	306.85 (552.33)	303.23 (545.82)	301.61 (542.90)	298.79 (537.82)
123	2449 (355.2)	3.19	2508 (8228)	98.4	495.54 (891.98)	485.41 (873.73)	467.16 (840.89)	337.87 (608.17)	320.36 (576.65)	311.32 (560.37)	308.63 (555.54)	306.82 (552.28)	304.47 (548.05)	301.49 (542.69)	300.77 (541.39)	298.31 (536.95)
124	2492 (361.4)	2.78	2543 (8342)	99.4	466.03 (838.85)	472.82 (851.08)	455.58 (820.05)	346.70 (624.06)	330.64 (595.15)	321.01 (577.82)	316.46 (569.63)	313.23 (563.81)	309.48 (557.07)	306.26 (551.27)	305.19 (549.34)	302.92 (545.26)
125	2441 (354.0)	3.74	2451 (8042)	97.2	548.57 (987.43)	491.74 (885.14)	472.26 (850.06)	362.29 (652.12)	344.47 (620.04)	331.29 (596.32)	325.07 (585.12)	320.82 (577.48)	315.92 (568.66)	311.80 (561.24)	310.01 (558.01)	306.73 (552.12)

TABLE VI.—EXPERIMENTALLY DETERMINED NOZZLE TEMPERATURES

Reading	Effective chamber pressure, $P_{c,e}$, kN/m^2 (psia)	Propellant mixture ratio, O/F	Characteristic exhaust velocity, C^*, m/sec (ft/sec)	Characteristic exhaust velocity efficiency, η_{C^*}, percent	Expansion area ratio, ϵ											
					5.6	12	20	50	100	200	300	388	500	635	800	975
					Heat flux to nozzle wall, kW/m^2 (Btu/m^2 sec)											
112	2482 (360.0)	3.84	2402 (7880)	95.5	962.6 (0.5890)	999.7 (0.6117)	693.4 (0.4243)	376.4 (0.2303)	197.1 (0.1206)	106.2 (0.0650)	72.2 (0.0442)	58.0 (0.0355)	44.3 (0.0271)	33.3 (0.0204)	26.1 (0.0160)	21.9 (0.0134)
113	2461 (356.9)	4.36	2346 (7697)	95.0	1043.6 (.6386)	1045.9 (.6400)	749.3 (.4585)	394.8 (.2416)	216.2 (.1323)	116.4 (.0712)	79.3 (.0485)	64.1 (.0392)	48.9 (.0299)	36.8 (.0225)	29.4 (.0180)	22.9 (.0140)
114	2488 (360.9)	5.08	2283 (7491)	94.4	1244.6 (.7616)	1104.3 (.6757)	800.8 (.4900)	435.0 (.2662)	240.1 (.1469)	127.1 (.0778)	85.5 (.0523)	69.8 (.0427)	54.6 (.0334)	41.2 (.0252)	29.6 (.0181)	22.9 (.0140)
115	2450 (355.3)	5.49	2244 (7363)	94.2	1211.8 (.7415)	1101.0 (.6737)	813.5 (.4978)	436.0 (.2668)	240.4 (.1471)	126.5 (.0774)	86.6 (.0530)	73.5 (.0450)	54.6 (.0334)	44.1 (.0270)	29.4 (.0180)	23.4 (.0143)
117	2456 (356.2)	3.19	2453 (8048)	96.4	703.1 (.4302)	740.6 (.4532)	537.2 (.3287)	265.1 (.1622)	142.0 (.0869)	78.3 (.0479)	53.9 (.0330)	46.7 (.0286)	36.0 (.0220)	27.3 (.0167)	20.9 (.0128)	19.3 (.0118)
120	2449 (355.2)	4.30	2377 (7799)	95.7	1178.9 (.7214)	812.2 (.4970)	626.4 (.3833)	348.1 (.2130)	211.8 (.1296)	116.2 (.0711)	76.6 (.0469)	65.2 (.0399)	47.7 (.0292)	34.5 (.0211)	25.0 (.0153)	19.0 (.0116)
121	2482 (360.0)	4.11	2418 (7934)	96.8	1009.6 (.6178)	716.5 (.4384)	614.8 (.3762)	364.6 (.2231)	207.9 (.1272)	108.7 (.0665)	72.9 (.0446)	60.8 (.0372)	45.6 (.0279)	33.3 (.0204)	23.4 (.0143)	18.3 (.0112)
123	2449 (355.2)	3.19	2508 (8228)	98.4	714.5 (.4372)	664.2 (.4064)	607.0 (.3714)	305.0 (.1866)	162.4 (.0994)	85.6 (.0524)	55.9 (.0342)	49.5 (.0303)	35.6 (.0218)	26.1 (.0160)	19.0 (.0116)	15.0 (.0092)
124	2492 (361.4)	2.78	2543 (8342)	99.4	604.5 (.3699)	603.4 (.3692)	542.4 (.3319)	276.2 (.1690)	142.2 (.0870)	77.8 (.0476)	51.0 (.0312)	45.8 (.0280)	31.5 (.0193)	23.2 (.0142)	17.8 (.0109)	16.7 (.0102)
125	2441 (354.0)	3.74	2451 (8042)	97.2	883.3 (.5405)	653.0 (.3996)	576.9 (.3530)	333.5 (.2041)	183.7 (.1124)	95.3 (.0583)	64.1 (.0392)	55.6 (.0340)	41.0 (.0251)	29.1 (.0178)	20.8 (.0127)	17.6 (.0108)

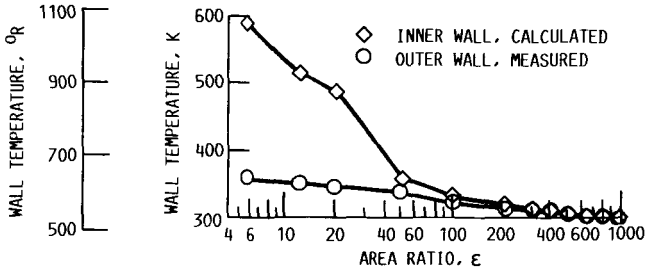

Figure 5.—Nozzle wall temperature distributions (reading 121).

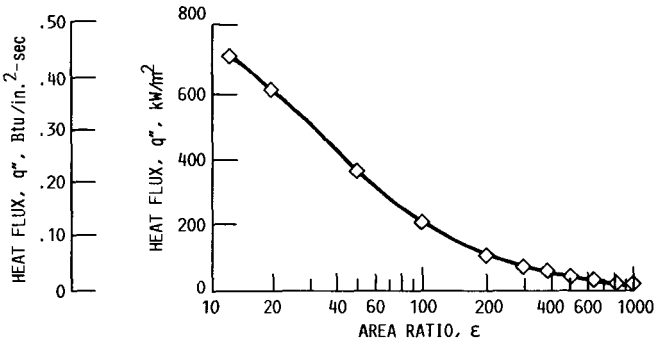

Figure 6.—Calculated nozzle wall heat-flux distribution (reading 121).

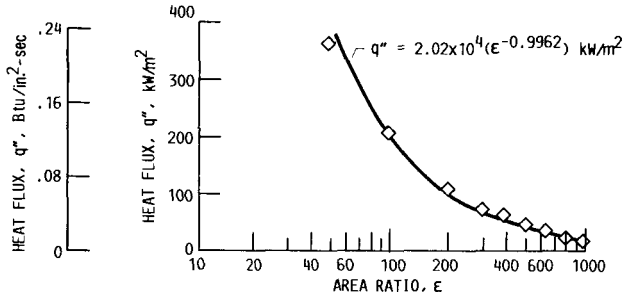

Figure 7.—Calculated nozzle wall heat-flux distribution for area ratios from 50 to 975 (reading 121).

In figure 5, the measured outer-wall temperatures and calculated inner-wall temperatures are presented for experimental reading 121. In figure 6, the variation of local heat flux with respect to area ratio is presented for the same reading. (It should be noted that calculations of heat flux and inner-wall temperature for the two lowest area ratio locations (area ratios of 5.6 and 12) are considered inaccurate because of the proximity of these locations to the water-cooled manifold.) As expected, the heat flux decreases with area ratio. In figure 7, the data is presented in consideration of only the higher area ratio data points (≥ 50). A best-fit curve to this data has the equation

$$q'' = B(\epsilon)^{-0.9962} \tag{8}$$

where $B = 2.02 \times 10^7$ W/m^2 (12.37 Btu/in.^{2} sec)

The curve appears to fit the experimental data, from an area ratio of 100 to 975, very well. Of course, such variables as chamber pressure, mixture ratio, characteristic velocity, and nozzle contour will significantly affect the heat-transfer rate and, hence, the correlation. Consequently, the calculation of heat flux at high area ratios is considerably more complex than indicated in equation (8).

The total amount of heat transferred from a rocket nozzle is often of interest, especially when a regeneratively cooled engine design is being considered. This total heat transfer, or heat rate, can be determined between two axial locations by calculating the area under the curve in figure 8. The points which make up this curve are the experimentally determined heat rate per unit of axial length for each thermocouple location. It is readily apparent from this figure that a significant amount of heat transfer occurs even in the high-area-ratio region. In figure 9, the same data are presented, but the points at area ratios of 5.6, 12, and 20 are omitted. A best-fit curve to this data has the equation

$$q'' = B\frac{(L^{-0.6702}\cos\theta)}{(2\pi R_i)} \tag{9}$$

where $B = 1.84 \times 10^5$ W/m^2 (16.261 Btu/in.^{2} sec)

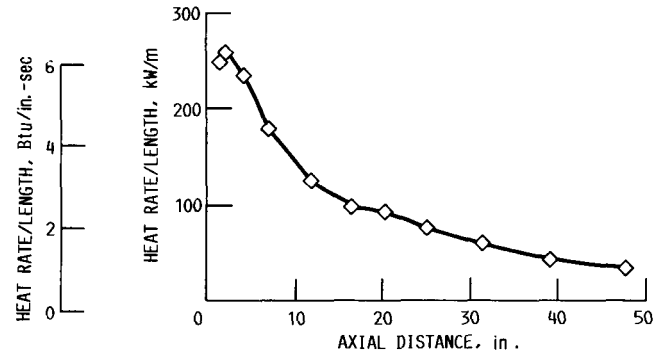

Figure 8.—Heat rate divided by length ($q''\pi D_i/\cos\theta$) as function of axial distance for area ratios from 12 to 975 (reading 121). Axial distance is measured from the throat.

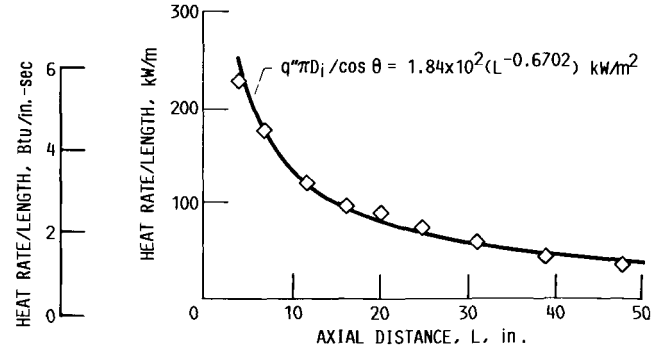

Figure 9.—Heat rate divided by length ($q''\pi D_i/\cos\theta$) as function of axial distance for area ratios from 50 to 975 (reading 121).

This equation was used to determine the heat-rate values over a specified length of the nozzle for each experimental reading. (The accuracy of using this procedure to calculate heat rate is evaluated in appendix D.) These experimentally obtained heat-rate results are compared to the predicted values and are presented in the following section.

Analytical Results

As previously mentioned, the December 1984 version of TDK was used to provide predictions of heat flux and heat rate. The discussion which follows compares the experimental and predicted results.

Figure 10 compares the experimental heat fluxes from reading 121 with the TDK-predicted heat fluxes. Because the TDK computer program does not account for energy-release losses, it assumes 100 percent combustion efficiency. Because the combustion efficiency for reading 121 was 96.79 percent, the experimental fluxes had to be adjusted to make a more accurate comparison. The equation used to adjust the fluxes was

$$q''_{\text{100 percent efficiency}} = \frac{q''}{(\eta_{C^*})^2} \tag{10}$$

The term $(\eta_{C^*})^2$ represents the adjustment for combustion efficiency based on C^* being proportional to the square root of the total chamber temperature. When the adjusted experimental and predicted values for area ratios from 20 to 975 are compared, the TDK predictions for a completely laminar boundary layer are within 15 percent of the experimental values. For the same area ratio range, the predictions for a turbulent boundary layer are approximately 120 percent higher. It should be noted that for the area ratios of 5.6 and 12 the laminar boundary-layer predictions are 87 and 29 percent higher, respectively, than the adjusted experimental results. The corresponding turbulent boundary-layer predictions are 319 and 246 percent higher, respectively. A possible explanation of this large discrepancy is a breakdown of the assumptions used in the experimental heat flux calculation due to the proximity of the water-cooled manifold.

Figure 11 presents the variation of heat rate Q with mixture ratio. Each data point corresponds to an experimental reading from table IV. The experimental values were obtained by calculating Q from area ratios of 140 to 1030 and adjusting those values for combustion efficiency as discussed previously. The theoretical values were calculated by using the TDK computer program and assuming a laminar boundary layer. Overall, the laminar predictions are within 13 percent of the experimental values.

The assumption of a completely laminar boundary layer within the 1030:1 nozzle appears to be substantiated by both

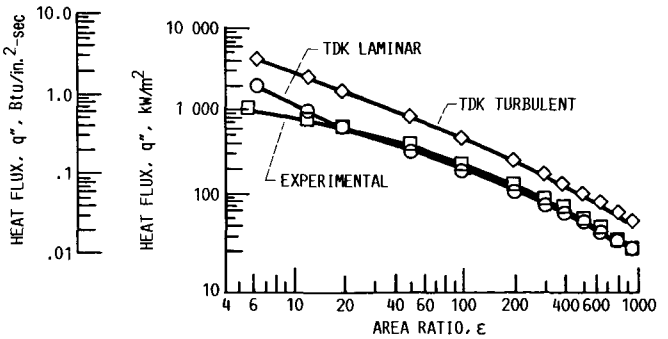

Figure 10.—Calculated (experimental) and predicted heat-flux distributions. Experimental values are corrected for characteristic exhaust velocity efficiency (reading 121).

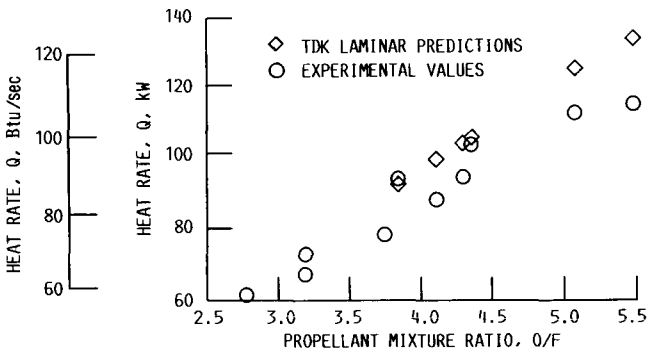

Figure 11.—Heat rate for area ratios from 140 to 1030 as function of mixture ratio.

figures 10 and 11. In figure 10, the experimental fluxes are slightly higher than the laminar predictions, but the difference between experiment and prediction decreases as the area ratio increases. If the boundary layer had transitioned to turbulent within the nozzle skirt, this difference would have become greater as the area ratio increased. In figure 11, the laminar predicted heat rates are all higher than their corresponding experimental values. Therefore, predicted heat rates for turbulent flow would be significantly larger than the experimental values. To support the predicted results, we performed a study to determine if the conditions within the nozzle were such that a laminar boundary layer could exist. The results of this study are presented in the next section.

Relaminarization Study

Relaminarization is the phenomena whereby a boundary layer reverts from turbulent flow to laminarlike flow. The importance of relaminarization in rocket nozzles results from the need to understand the structure of the boundary layer in the nozzle and thereby the heat transfer across the boundary layer. If a boundary layer relaminarizes, there will be a reduction in heat transfer.

Relaminarization is believed to be associated with the effect of flow acceleration on turbulence. For a given rocket nozzle

contour, the parameter which appears to be most strongly related to relaminarization is chamber pressure. Back, Cuffel, and Massier (ref. 9) obtained boundary-layer and heat-transfer measurements for flow through a cooled, conical nozzle at various chamber pressures. At the lower chamber pressures, they found heat transfer was reduced by as much as 50 percent along the convergent section. They also found that when the acceleration parameter K exceeded about 2×10^{-6}, where

$$K = \left(\frac{\mu_e}{\rho_e u_e^2}\right)\frac{du_e}{dx} \tag{11}$$

heat transfer was reduced below values typical of turbulent boundary layers.

In another study done by Boldman, Schmidt, and Gallagher (ref. 10) heat-transfer measurements were obtained at various chamber pressures in a cooled nozzle. At the lower chamber pressures, the authors measured a depression in heat transfer from the predicted values for turbulent pipe flow. An axisymmetric acceleration parameter was derived from the integral momentum equation based on a critical momentum-thickness Reynolds number of 360. It was found that when this axisymmetric acceleration parameter K_{ax} exceeded a value of 2.88×10^{-6}, where

$$K_{ax} = \frac{\nu_\infty}{u_\infty^2}\frac{du_\infty}{dx} + 0.352\left(\frac{\nu_\infty}{u_\infty r}\right)\frac{dr}{dx} \tag{12}$$

there was a reduction in heat transfer.

Currently, work is being done under contract from NASA Marshall Space Flight Center to improve the BLIMP-J computer code (ref. 11). Specifically, one of the improvements being made to BLIMP-J is the incorporation of the acceleration parameter K into the program as a criteria for relaminarization. Previously, the BLIMP-J code only used the criteria of $Re_\theta = 360$ as an indication of transition from laminar to turbulent flow.

Initially, to determine if the predicted flow conditions within the 1030:1 nozzle caused transition of the flow from laminar to turbulent, we calculated the momentum-thickness Reynolds number using the inviscid TDK results and the momentum thickness predicted for a laminar boundary layer. Although the BLIMP-J code uses a transition criteria of $Re_\theta = 360$, others predict that for compressible flow with a pressure gradient the criteria should be approximately $Re_\theta = 400$ (ref. 6, p. 332). Figure 12 shows predictions of the momentum-thickness Reynolds number along the nozzle. As indicated by the horizontal line of $Re_\theta = 400$, the predicted conditions imply that if transition did occur, it would occur at the throat and slightly beyond.

Next, the acceleration parameters K and K_{ax} were calculated for the flow along the nozzle using inviscid TDK results. In figure 13, the acceleration parameter K exceeds the critical value of 2.0×10^{-6} before the throat and at the throat. In figure 14, the acceleration parameter K_{ax} exceeds its critical values of 2.88×10^{-6} at the throat and slightly beyond. Since K_{ax} exceeds the critical value in the convergence and throat region, one would expect relaminarization of the flow in this region. Although the values of K_{ax} lie below the critical value for the remainder of the nozzle, the momentum-thickness Reynolds number shown in figure 12 indicates the flow beyond the throat would not be inclined to transition to turbulent until near the exit plane of the nozzle.

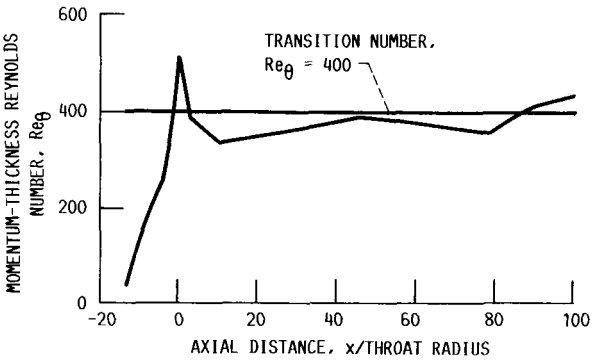

Figure 12.—Momentum-thickness Reynolds number Re_θ as function of axial distance divided by throat radius (reading 121).

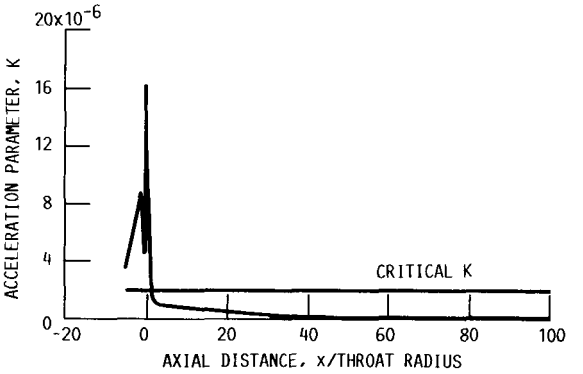

Figure 13.—Acceleration parameter K as function of axial distance divided by throat radius (reading 121).

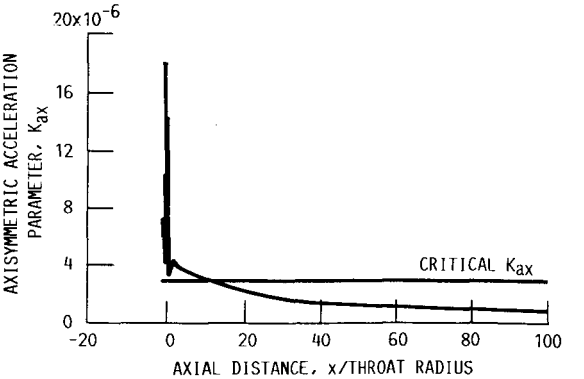

Figure 14.—Axisymmetric acceleration parameter K_{ax} as function of axial distance divided by throat radius (reading 121).

Summary of Results

Outer-wall temperature measurements were taken from a 1030:1 carbon steel rocket nozzle tested at the NASA Lewis Research Center Rocket Engine Test Facility. The heat-sink nozzle was tested using gaseous oxygen and gaseous hydrogen propellants. The nominal chamber pressure was 2413 kN/m^2 (350 psia), and the mixture ratio range was 2.78 to 5.49.

The following results were obtained:

1. Inner-wall temperatures and heat fluxes were obtained by using experimentally measured nozzle outer-wall temperatures.

2. From the calculated heat fluxes, heat rates to the nozzle wall at specified axial locations were determined.

3. The experimentally determined heat fluxes were compared with those predicted by the TDK computer analysis program. For turbulent boundary-layer flow in the nozzle, the predicted heat fluxes were 120 percent higher than the experimental heat fluxes for area ratios from 20 to 975. The corresponding predictions for laminar boundary-layer flow were within 15 percent of the experimental values.

4. Based on the comparison of experimental and predicted results, we concluded that there was laminar boundary-layer flow within the 1030:1 nozzle.

5. To support the prediction of laminar boundary-layer flow, a study was performed to examine the flow conditions. The results of the study indicated that the acceleration of the flow within the nozzle, combined with the low-momentum-thickness Reynolds number conditions, supports the existence of laminarlike boundary-layer flow.

Lewis Research Center
National Aeronautics and Space Administration
Cleveland, Ohio, May 19, 1987

Appendix A
Inner-wall Temperature and Heat Flux Solution

The solution of the equation

$$\rho C_v \frac{\partial T}{\partial t} = \frac{1}{r}\frac{\partial}{\partial r}\left(kr\frac{\partial T}{\partial r}\right) \tag{A1}$$

will be presented assuming

(1) Constant properties
(2) Linear rate of temperature rise
(3) Adiabatic outer wall
(4) No axial or circumferential conduction

Then,

$$\frac{1}{\alpha}\frac{\partial T}{\partial t} = \frac{1}{r}\frac{\partial}{\partial r}\left(r\frac{\partial T}{\partial r}\right) \tag{A2}$$

Since $\partial T/\partial t$ is independent of position, integration yields

$$T = \frac{r^2}{4\alpha}\frac{\partial T}{\partial t} + c_1 \ln r + c_2 \tag{A3}$$

where it is recognized that c_1 and c_2 can be functions of time.

The following boundary conditions apply:

(1) At $r = R_o$, $\partial T/\partial r = 0$ (adiabatic)
(2) At $r = R_o$, $T = T_o(t)$

The solution equation (A3) yields

$$T = T_o(t) - \frac{R_o^2}{4\alpha}\frac{\partial T}{\partial t}\left[1 - \left(\frac{r}{R_o}\right)^2\right] - \frac{R_o^2}{2\alpha}\frac{\partial T}{\partial t}\ln\left(\frac{r}{R_o}\right) \tag{A4}$$

The inner-wall temperature at a given time is

$$T_i = T_o - \frac{R_o^2}{4\alpha}\frac{\partial T}{\partial t}\left[1 - \left(\frac{R_i}{R_o}\right)^2\right] - \frac{R_o^2}{4\alpha}\frac{\partial T}{\partial t}\ln\left(\frac{R_i}{R_o}\right)^2 \tag{A5}$$

for a single material system. And the inner-wall heat flux is

$$q_i'' = \frac{kR_i}{2\alpha}\left(\frac{\partial T}{\partial t}\right)\left[\left(\frac{R_o}{R_i}\right)^2 - 1\right] \tag{A6}$$

for a single material system.

The preceding solution for temperature and heat flux (eqs. (A5) to (A6)) can be used as boundary conditions for a two-material system (let $R_i = R_z$). That is, at the interface,

$$T_1 = T_o - \frac{R_o^2}{4\alpha_1}\left(\frac{\partial T}{\partial t}\right)\left[1 - \left(\frac{R_z}{R_o}\right)^2\right]$$

$$- \frac{R_o^2}{4\alpha_1}\left(\frac{\partial T}{\partial t}\right)\ln\left(\frac{R_z}{R_o}\right)^2 = T_2 \tag{A7}$$

$$q_1'' = \frac{k_1 R_z}{2\alpha_1}\left(\frac{\partial T}{\partial t}\right)\left[\left(\frac{R_o}{R_z}\right)^2 - 1\right] = -k_2\frac{\partial T_2}{\partial r} = q_2'' \quad \text{(A8)}$$

where subscript 1 indicates the outer material and subscript 2 indicates the inner material.

As the interface temperature of both materials must be equal, the time response of both materials $\partial T/\partial t$ must be equal. Then, the solution becomes

$$T = T_o + \frac{r^2}{4\alpha_2}\left(\frac{\partial T}{\partial t}\right) - \frac{R_z^2}{2\alpha_1}\left(\frac{\partial T}{\partial t}\right) \times \left\{\frac{k_1}{k_2}\left[\left(\frac{R_o}{R_z}\right)^2 - 1\right] + \frac{\alpha_1}{\alpha_2}\right\}\ln r - \left\{\frac{R_o^2}{4\alpha_1}\left(\frac{\partial T}{\partial t}\right) \times \left[1 - \left(\frac{R_z}{R_o}\right)^2 + \ln\left(\frac{R_z}{R_o}\right)^2\right]\right\} - \frac{R_z^2}{4\alpha_2}\left(\frac{\partial T}{\partial t}\right) + \frac{R_z^2}{2\alpha_1}\left(\frac{\partial T}{\partial t}\right)\left\{\frac{k_1}{k_2}\left[\left(\frac{R_o}{R_z}\right)^2 - 1\right] + \frac{\alpha_1}{\alpha_2}\right\}\ln R_z \quad \text{(A9)}$$

Therefore, from equation (A9), the inner-wall conditions at a given time for a two-material system are

$$T_i = T_o - \frac{R_i^2}{4\alpha_2}\left(\frac{\partial T}{\partial t}\right)\left[\left(\frac{R_z}{R_i}\right)^2 - 1\right] - \left\{\frac{R_o^2}{4\alpha_1}\left(\frac{\partial T}{\partial t}\right) \times \left[1 - \left(\frac{R_z}{R_o}\right)^2 + \ln\left(\frac{R_z}{R_o}\right)^2\right]\right\} - \left\{\frac{R_z^2}{2\alpha_1}\left(\frac{\partial T}{\partial t}\right) \times \frac{k_1}{k_2}\left[\left(\frac{R_o}{R_z}\right)^2 - 1 + \frac{k_2}{k_1}\frac{\alpha_1}{\alpha_2}\right]\ln\left(\frac{R_i}{R_z}\right)\right\} \quad \text{(A10)}$$

and

$$q_i'' = \frac{k_2 R_i\left(\frac{\partial T}{\partial t}\right)}{2\alpha_2} \left\{\left(\frac{R_z}{R_i}\right)^2\frac{\alpha_2 k_i}{\alpha_1 k_2}\left[\left(\frac{R_o}{R_z}\right)^2 - 1 + \frac{\alpha_1 k_2}{\alpha_2 k_1}\right] - 1\right\} \quad \text{(A11)}$$

Equations (A10) and (A11) can be simplified to the forms

$$T_i = T_o + \frac{\left(\frac{\partial T}{\partial t}\right)}{4\alpha_2}\left(R_i^2 - R_z^2\right) + \left\{\frac{\left(\frac{\partial T}{\partial t}\right)}{4\alpha_1}\left[R_z^2 - R_o^2 - R_o^2\ln\left(\frac{R_z}{R_o}\right)^2\right]\right\} + \frac{\left(\frac{\partial T}{\partial t}\right)k_1}{2\alpha_1 k_2}\left(\ln\frac{R_i}{R_z}\right)\left(R_z^2 - R_o^2 - R_z^2\frac{\alpha_1 k_2}{\alpha_2 k_1}\right) \quad \text{(A12)}$$

and

$$q_i'' = \frac{\left(\frac{\partial T}{\partial t}\right)k_1}{2R_i\alpha_1}\left(R_o^2 - R_z^2\right) + \frac{\left(\frac{\partial T}{\partial t}\right)k_2}{2\alpha_2 R_i}\left(R_z^2 - R_i^2\right) \quad \text{(A13)}$$

Appendix B
Examination of Assumptions

An order-of-magnitude analysis can be applied to examine the accuracy of the following assumptions:

(1) No axial heat transfer

(2) No heat transfer from the outer wall

Axial Heat Transfer

If axial conduction is to be considered, the governing differential equation becomes

$$\frac{1}{\alpha}\frac{\partial T}{\partial t} = \frac{1}{r}\frac{\partial}{\partial r}\left(r\frac{\partial T}{\partial r}\right) + \frac{\partial^2 T}{\partial x^2}$$

If $\partial^2 T/\partial x^2 << (1/\alpha)\,(\partial T/\partial t)$, then axial conduction may be reasonably neglected. The axial conduction term may be approximated as

$$\frac{\partial^2 T_n}{\partial x^2} \simeq \frac{T_{n+1} - 2T_n + T_{n-1}}{(\Delta \bar{x})^2}$$

The subscripts $n+1$, n, and $n-1$ represent outer-wall thermocouple locations. An experimental evaluation of the ratio

$$\frac{\partial^2 T}{\partial x^2} \Big/ \left(\frac{1}{\alpha}\frac{\partial T}{\partial t}\right)$$

using the experimental data from a typical performance reading is presented in figure 15. Axial conduction accounts for less than 2 percent of the transient term.

Radiation Heat Transfer

The amount of heat loss due to radiation from the outer nozzle wall can be estimated as

$$q_R'' \simeq \sigma(T^4 - T_a^4)$$

where q_R is the heat flux due to radiation, σ the Stefan-Boltzman constant, and T_a the ambient temperature.

An experimental evaluation of the ratio of q_R''/q_{Adia} is presented in figure 15 using the data from a typical experimental reading. The parameter q_{Adia} represents the heat flux for an adiabatic outer wall condition. It can be seen that radiation heat transfer is relatively low (<1 percent) as compared to total heat transfer.

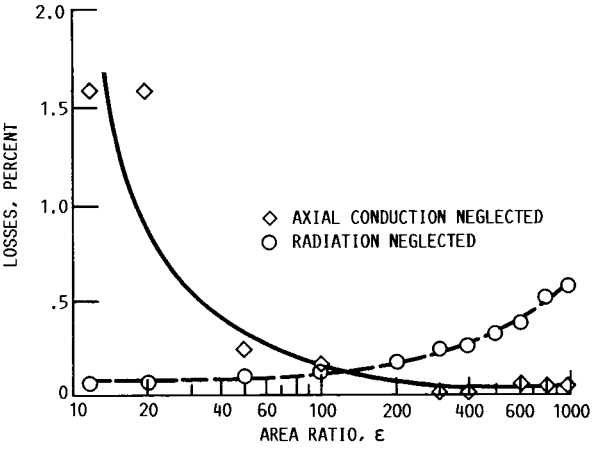

Figure 15.—Estimation of axial conduction and radiation losses.

Appendix C
TDK Input Files

Input for Reading 112

```
LOW T CPHS
H                    2
100.       4.968                          1
200.       4.968                          2
H2                   2
100.       6.729                          1
200.       6.560                          2
H2O                  2
100.       7.961                          1
200.       7.969                          2
O                    2
100.       5.665                          1
200.       5.433                          2
OH                   2
100.       7.798                          1
200.       7.356                          2
O2                   2
100.       6.956                          1
200.       6.961                          2
END LOW T CPHS
TITLE  HIGH E NOZZLE STUDY: E=1000 AND READING = 112
DATA
 &DATA
  ODE=1,ODK=1,TDK=1,BLM=1,IRPEAT=2,IOFF=6,
   RSI=0.5,ASUB=3.,1.5,NASUB=2,IRSTRT=0,
   ASUP=1.5,2.0,30.0,200.0,400.0,600.0,1024.0,NASUP=7,
   ECRAT=4.223,RI=2.,THETAI=25.,RWTU=2.,
```

```
   ITYPE=0,IWALL=4,RWTD=0.4,THETA=39.41,
   THE=7.94,NWS=36,
  RS=   0.0000,    1.1316,    1.1780,    1.2748,
        1.3704,    1.4198,    1.7658,    2.0876,
     2.4916,    3.0372,    5.2522,       5.7028,
        6.5606,    7.0420,    7.5072,    8.0464,
     9.0636,    9.5394,    10.6852,   12.0244,
    12.7284,     14.0056,   15.2408,   15.9610,
    16.6554,   17.3210,   18.7560,   19.6768,   20.5562,
    21.6918,   23.7554,   24.6744,    27.0428,
    29.1286,   30.1862,  32.0156,
  ZS=   0.0000,    0.3094,    0.3654,    0.4778,
        0.5908,    0.6480,    1.0430,    1.4050,
     1.8722,    2.5246,    5.5320,       6.2150,
        7.5802,    8.3862,    9.1920,   10.1592,
    12.0810,   13.0230,     15.4056,   18.4006,
    20.0684,     23.2606,   26.5588,   28.5824,
    30.6060,   32.6136,   37.1806,   40.2916,   43.4026,
    47.6334,   55.9914,   60.0166,   71.3698,
    82.7063,   89.0425,   101.2383,
 &END
REACTANTS
H 2.                                    00        100.              G285.60  F
O 2.                                    00        100.              G279.20  O

NAMELISTS
 &ODE
  RKT=T,P=360.0,PSIA=T,OF=T,OFSKED=3.84,
   SUPAR=30.0,200.0,400.0,600.0,1024.0,ECRAT=4.223,
 &END
REACTIONS
  H + OH = H2O        , A=8.4E21 , N=2.0   , B=0.,   (AR) BAULCH 72 (A) 1OU
  O + H  = OH         , A=3.62E18 , N=1.    , B=0.,   (AR) JENSEN 78 (B) 3OU
  O + O  = O2         , A=1.9E13 , N=0.    , B=-1.79,  (AR) BAULCH 76 (A) 1OU
  H + H  = H2         , A=6.4E17 , N=1.    , B=0.,   (AR) BAULCH 72 (A) 3OU
END TBR REAX
  H2 + OH = H2O + H , A=2.20E13,  N=0.00,  B=5.15,  BAULCH 72 (A) 2U
  OH + OH =  H2O + O , A=6.30E12,  N=0.00,  B= 1.09,  BAULCH 72 (A) 3U
  H2 + O = H + OH   , A=1.80E10, N=-1.   , B=8.9,   BAULCH 72 (A) 1.5U
  O2 + H = O + OH   , A=2.2E14 , N=0.    , B=16.8,  BAULCH 72 (A) 1.5U
LAST REAX
THIRD BODY REAX RATE RATIOS
SPECIES H2,5.,5.,5.,4.,
SPECIES H2O,17.,5.,5.,10.,
SPECIES O2,6.,5.,11.,1.5,
SPECIES H,12.5,12.5,12.5,25.,
SPECIES O,12.5,12.5,12.5,25.,
SPECIES OH,12.5,12.5,12.5,25.,
LAST CARD
 &ODK
  EP=0.0,JPRNT=-2,MAVISP=1,XM(1)=1.0,NJPRNT=7,
   HI=0.01,HMIN=0.01,HMAX=0.01,
 &END
 &TRANS
  MP=200,
 &END
 &MOC
  EXITPL=.FALSE.,EPW=0.05,
 &END
 &BLM
  IHFLAG=0,NTQW=19,
  TQW=1260.0,1260.0,1260.0,2770.0,3330.0,3960.0,4050.0,
    1008.61,1039.24,886.05,610.30,571.14,549.45,
    528.76,538.35,520.14,530.12,516.42,525.62,
  XTQW=  -13.0,-6.0,-2.26,-2.14,-1.57,-0.89,0.0,
     1.8722,3.06,4.406,8.4344,13.9624,
    23.6164,32.6124,40.3644,50.2504,62.4584,77.9624,95.7704,
  APROF=30.,200.,400.0,1009.0,NPROF=4,KDTPLT=1,
   KMTPLT=1,KTWPLT=1,XSEG=-14.0,10.0,33.0,56.0,79.0,101.23,NSEGS=5,
   XINO(1)=-14.0,-12.0,-10.0,-8.0,-6.0,-4.0,
   RINO(1)=2.054,2.054,2.054,2.054,2.054,2.054,
   UEO(1)=81.0,216.0,351.0,486.0,621.0,757.0,
```

```
   TEO(1)=5450.0,5449.6,5448.4,5446.2,5444.0,5442.8,
   PEO(1)=360.0,359.6,358.3,357.65,356.0,355.9,
   NTR=700,
 &END
```

Input for Reading 113

```
LOW T CPHS
H                    2
100.       4.968                              1
200.       4.968                              2
H2                   2
100.       6.729                              1
200.       6.560                              2
H2O                  2
100.       7.961                              1
200.       7.969                              2
O                    2
100.       5.665                              1
200.       5.433                              2
OH                   2
100.       7.798                              1
200.       7.356                              2
O2                   2
100.       6.956                              1
200.       6.961                              2
END LOW T CPHS
TITLE  HIGH E NOZZLE STUDY: E=1000 AND READING = 113
DATA
 &DATA
  ODE=1,CDK=1,TDK=0,BLM=0,IRPEAT=0,IOFF=6,
   RSI=0.5,ASUB=3.,1.5,NASUB=2,IRSTRT=0,
   ASUP=1.5,2.0,30.0,200.0,400.0,600.0,1024.0,NASUP=7,
   ECRAT=4.223,RI=2.,THETAI=25.,RWTU=2.,
   ITYPE=0,IWALL=4,RWTD=0.4,THETA=39.41,
   THE=7.94,NWS=36,
  RS=   0.0000,    1.1316,   1.1780,   1.2748,
        1.3704,   1.4198,   1.7658,   2.0876,
     2.4916,   3.0372,   5.2522,       5.7028,
        6.5606,   7.0420,   7.5072,   8.0464,
     9.0636,   9.5394,    10.6852,  12.0244,
    12.7284,    14.0056,  15.2408,  15.9610,
    16.6554,  17.3210,  18.7560,  19.6768,  20.5562,
    21.6918,  23.7554,  24.6744,   27.0428,
    29.1286,  30.1862, 32.0156,
  ZS=  0.0000,    0.3094,   0.3654,   0.4778,
        0.5908,   0.6480,   1.0430,   1.4050,
     1.8722,   2.5246,   5.5320,       6.2150,
        7.5802,   8.3862,   9.1920,  10.1592,
    12.0810,  13.0230,    15.4056,  18.4006,
    20.0684,    23.2606,  26.5588,  28.5824,
    30.6060,  32.6136,  37.1806,  40.2916,  43.4026,
    47.6334,  55.9914,  60.0166,  71.3698,
    82.7063,  89.0425,  101.2383,
 &END
REACTANTS
H 2.                                    00        100.              G284.20  F
O 2.                                    00        100.              G277.00  O
NAMELISTS
 &ODE
  RKT=T,P=356.9,PSIA=T,OF=T,OFSKED=4.36,
   SUPAR=30.0,200.0,400.0,600.0,1024.0,ECRAT=4.223,
 &END
REACTIONS
  H + OH = H2O        , A=8.4E21 , N=2.0  , B=0.,  (AR) BAULCH 72 (A) 10U
  O + H  = OH         , A=3.62E18 , N=1.   , B=0.,  (AR) JENSEN 78 (B) 30U
  O + O  = O2         , A=1.9E13 , N=0.   , B=-1.79,  (AR) BAULCH 76 (A) 10U
  H + H  = H2         , A=6.4E17 , N=1.   , B=0.,  (AR) BAULCH 72 (A) 30U
END TBR REAX
  H2 + OH = H2O + H , A=2.20E13,  N=0.00,  B=5.15,  BAULCH 72 (A) 2U
  OH + OH =  H2O + O , A=6.30E12,  N=0.00,  B= 1.09,  BAULCH 72 (A) 3U
```

```
  H2 + O = H + OH    , A=1.80E10, N=-1.   , B=8.9,    BAULCH 72 (A) 1.5U
  O2 + H = O + OH    , A=2.2E14 , N=0.    , B=16.8,   BAULCH 72 (A) 1.5U
LAST REAX
THIRD BODY REAX RATE RATIOS
SPECIES H2,5.,5.,5.,4.,
SPECIES H2O,17.,5.,5.,10.,
SPECIES O2,6.,5.,11.,1.5,
SPECIES H,12.5,12.5,12.5,25.,
SPECIES O,12.5,12.5,12.5,25.,
SPECIES OH,12.5,12.5,12.5,25.,
LAST CARD
 &ODK
  EP=10.0,JPRNT=-2,MAVISP=1,XM(1)=1.0,NJPRNT=7,
   HI=0.01,HMIN=0.01,HMAX=0.01,
 &END
 &TRANS
  MP=200,
 &END
 &MOC
  EXITPL=.FALSE.,EPW=0.05,
 &END
 &BLM
  IHFLAG=0,NTQW=19,
  TQW=1260.0,1260.0,1260.0,2770.0,3330.0,3960.0,4050.0,
    1061.73,1080.00,934.61,641.91,600.62,574.11,
    551.50,555.18,536.63,541.40,528.52,533.44,
  XTQW=  -15.0,-6.0,-2.26,-2.14,-1.57,-0.89,0.0,
     1.8722,3.06,4.406,8.4344,13.9624,
    23.6164,32.6124,40.3644,50.2504,62.4584,77.9624,95.7704,
  APROF=30.,200.,400.0,1009.0,NPROF=4,KDTPLT=1, NTR=700,
   KMTPLT=1,KTWPLT=1,XSEG=-14.0,10.0,33.0,56.0,79.0,101.23,NSEGS=5,
   XINO(1)=-14.0,-12.0,-10.0,-8.0,-6.0,-4.0,
   RINO(1)=2.054,2.054,2.054,2.054,2.054,2.054,
   UEO(1)=80.0,213.0,346.0,480.0,613.0,746.0,
   TEO(1)=5731.8,5731.0,5729.7,5728.2,5726.0,5724.8,
   PEO(1)=356.9,356.0,355.3,354.65,353.0,352.9,
 &END
```

Input for Reading 114

```
LOW T CPHS
H                    2
100.       4.968                              1
200.       4.968                              2
H2                   2
100.       6.729                              1
200.       6 560                              2
H2O                  2
100.       7.961                              1
200.       7.969                              2
O                    2
100.       5.665                              1
200.       5.433                              2
OH                   2
100.       7.798                              1
200.       7.356                              2
O2                   2
100.       6.956                              1
200.       6.961                              2
END LOW T CPHS
TITLE  HIGH E NOZZLE STUDY: E=1000 AND READING = 114
DATA
 &DATA
  ODE=1,ODK=1,TDK=1,BLM=1,IRPEAT=2,IOFF=6,
   RSI=0.5,ASUB=3.,1.5,NASUB=2,IRSTRT=0,
   ASUP=1.5,2.0,30.0,200.0,400.0,600.0,1024.0,NASUP=7,
   ECRAT=4.223,RI=2.,THETAI=25.,RWTU=2.,
   ITYPE=0,IWALL=4,RWTD=0.4,THETA=39.41,
   THE=7.94,NWS=36,
  RS=   0.0000,    1.1316,    1.1780,    1.2748,
```

```
      1.3704,   1.4198,   1.7658,   2.0876,
    2.4916,   3.0372,   5.2522,       5.7028,
      6.5606,   7.0420,   7.5072,   8.0464,
    9.0636,   9.5394,   10.6852,  12.0244,
   12.7284,    14.0056,  15.2408,  15.9610,
   16.6554,  17.3210,  18.7560,  19.6768,  20.5562,
   21.6918,  23.7554,  24.6744,   27.0428,
   29.1286,  30.1862, 32.0156,
  ZS=  0.0000,    0.3094,   0.3654,   0.4778,
       0.5908,   0.6480,   1.0430,   1.4050,
    1.8722,   2.5246,   5.5320,       6.2150,
       7.5802,   8.3862,   9.1920,  10.1592,
   12.0810,  13.0230,    15.4056,  18.4006,
   20.0684,    23.2606,  26.5588,  28.5824,
   30.6060,  32.6136,  37.1806,  40.2916,  43.4026,
   47.6334,  55.9914,  60.0166,  71.3698,
   82.7063,  89.0425,  101.2383,
 &END
REACTANTS
H 2.                                    00        100.     0.0       G283.90  F
O 2.                                    00        100.     0.0       G275.80  O

NAMELISTS
 &ODE
  RKT=T,P=360.9,PSIA=T,OF=T,OFSKED=5.08,
   SUPAR=30.0,200.0,400.0,600.0,1024.0,ECRAT=4.223,
 &END
REACTIONS
  H + OH = H2O        , A=8.4E21 , N=2.0   , B=0.,   (AR) BAULCH 72 (A) 10U
  O + H  = OH         , A=3.62E18 , N=1.    , B=0.,   (AR) JENSEN 78 (B) 30U
  O + O  = O2         , A=1.9E13 , N=0.    , B=-1.79,  (AR) BAULCH 76 (A) 10U
  H + H  = H2         , A=6.4E17 , N=1.    , B=0.,   (AR) BAULCH 72 (A) 30U
END TBR REAX
  H2 + OH = H2O + H , A=2.20E13,  N=0.00,  B=5.15,  BAULCH 72 (A) 2U
  OH + OH =  H2O + O , A=6.30E12,  N=0.00,  B= 1.09,  BAULCH 72 (A) 3U
  H2 + O = H + OH    , A=1.80E10, N=-1.   , B=8.9,    BAULCH 72 (A) 1.5U
  O2 + H = O + OH    , A=2.2E14 , N=0.    , B=16.8,   BAULCH 72 (A) 1.5U
LAST REAX
THIRD BODY REAX RATE RATIOS
SPECIES H2,5.,5.,5.,4.,
SPECIES H2O,17.,5.,5.,10.,
SPECIES O2,6.,5.,11.,1.5,
SPECIES H,12.5,12.5,12.5,25.,
SPECIES O,12.5,12.5,12.5,25.,
SPECIES OH,12.5,12.5,12.5,25.,
LAST CARD
 &ODK
  EP=0.0,JPRNT=-2,MAVISP=1,XM(1)=1.0,NJPRNT=7,
   HI=0.01,HMIN=0.01,HMAX=0.01,
 &END
 &TRANS
  MP=200,
 &END
 &MOC
  EXITPL=.FALSE.,EPW=0.05,
 &END
 &BLM
  IHFLAG=0,NTQW=17,
  TQW=1260.0,2770.0,3330.0,3960.0,4050.0,
    1169.58,1128.31,972.62,663.76,618.64,589.39,
    567.31,569.98,548.78,549.66,535.97,537.46,
  XTQW=  -2.26,-2.14,-1.57,-0.89,0.0,
     1.8722,3.06,4.406,8.4344,13.9624,
    23.6164,32.6124,40.3644,50.2504,62.4584,77.9624,95.7704,
  APROF=30.,200.,400.0,1009.0,NPROF=4,KDTPLT=1,
   KMTPLT=1,KTWPLT=1,XSEG=-14.0,10.0,33.0,56.0,79.0,101.23,NSEGS=5,
   XINO(1)=-14.0,-12.0,-10.0,-8.0,-6.0,-4.0,
   RINO(1)=2.054,2.054,2.054,2.054,2.054,2.054,
   UEO(1)=35.0,165.0,300.0,425.0,560.0,685.0,
   TEO(1)=6014.8,6013.6,6012.4,6011.2,6010.0,6008.8,
   PEO(1)=360.7,360.0,359.3,358.65,358.0,357.3,
   NTR=800,
 &END
```

Input for Reading 115

```
LOW T CPHS
H                    2
100.       4.968                                  1
200.       4.968                                  2
H2                   2
100.       6.729                                  1
200.       6.560                                  2
H2O                  2
100.       7.961                                  1
200.       7.969                                  2
O                    2
100.       5.665                                  1
200.       5.433                                  2
OH                   2
100.       7.798                                  1
200.       7.356                                  2
O2                   2
100.       6.956                                  1
200.       6.961                                  2
END LOW T CPHS
TITLE  HIGH E NOZZLE STUDY: E=1000 AND READING = 115
DATA
 &DATA
  ODE=1,ODK=1,TDK=1,BLM=1,IRPEAT=2,IOFF=6,
   RSI=0.5,ASUB=3.,1.5,NASUB=2,IRSTRT=2,
   ASUP=1.5,2.0,30.0,200.0,400.0,600.0,1024.0,NASUP=7,
   ECRAT=4.223,RI=2.,THETAI=25.,RWTU=2.,
   ITYPE=0,IWALL=4,RWTD=0.4,THETA=39.41,
   THE=7.94,NWS=36,
  RS=   0.0000,    1.1316,   1.1780,   1.2748,
        1.3704,   1.4198,   1.7658,   2.0876,
     2.4916,   3.0372,   5.2522,      5.7028,
        6.5606,   7.0420,   7.5072,   8.0464,
     9.0636,   9.5394,    10.6852,  12.0244,
    12.7284,    14.0056,  15.2408,  15.9610,
    16.6554,  17.3210,  18.7560,  19.6768,  20.5562,
    21.6918,  23.7554,  24.6744,   27.0428,
    29.1286,  30.1862, 32.0156,
  ZS=  0.0000,    0.3094,   0.3654,   0.4778,
        0.5908,   0.6480,   1.0430,   1.4050,
     1.8722,   2.5246,   5.5320,      6.2150,
        7.5802,   8.3862,   9.1920,  10.1592,
    12.0810,  13.0230,    15.4056,  18.4006,
    20.0684,    23.2606,  26.5588,  28.5824,
    30.6060,  32.6136,  37.1806,  40.2916,  43.4026,
    47.6334,  55.9914,  60.0166,  71.3698,
    82.7063,  89.0425,  101.2383,
 &END
REACTANTS
H 2.                                    00       100.            G283.50  F
O 2.                                    00       100.            G275.90  O

NAMELISTS
 &ODE
  RKT=T,P=355.3,PSIA=T,OF=T,OFSKED=5.49,
   SUPAR=30.0,200.0,400.0,600.0,1024.0,ECRAT=4.223,
 &END
REACTIONS
  H + OH = H2O       , A=8.4E21 , N=2.0  , B=0.,  (AR) BAULCH 72 (A) 10U
  O + H  = OH        , A=3.62E18 , N=1.   , B=0.,  (AR) JENSEN 78 (B) 30U
  O + O  = O2        , A=1.9E13 , N=0.   , B=-1.79,  (AR) BAULCH 76 (A) 10U
  H + H  = H2        , A=6.4E17 , N=1.   , B=0.,  (AR) BAULCH 72 (A) 30U
END TBR REAX
  H2 + OH = H2O + H , A=2.20E13,  N=0.00,  B=5.15,  BAULCH 72 (A) 2U
  OH + OH =  H2O + O , A=6.30E12,  N=0.00,  B= 1.09,  BAULCH 72 (A) 3U
  H2 + O = H + OH   , A=1.80E10, N=-1.  , B=8.9,   BAULCH 72 (A) 1.5U
  O2 + H = O + OH   , A=2.2E14 , N=0.   , B=16.8,  BAULCH 72 (A) 1.5U
LAST REAX
```

```
THIRD BODY REAX RATE RATIOS
SPECIES H2,5.,5.,5.,4.,
SPECIES H2O,17.,5.,5.,10.,
SPECIES O2,6.,5.,11.,1.5,
SPECIES H,12.5,12.5,12.5,25.,
SPECIES O,12.5,12.5,12.5,25.,
SPECIES OH,12.5,12.5,12.5,25.,
LAST CARD
 &ODK
  EP=0.0,JPRNT=-2,MAVISP=1,XM(1)=1.0,NJPRNT=7,
   HI=0.01,HMIN=0.01,HMAX=0.01,
 &END
 &TRANS
  MP=200,
 &END
 &MOC
  EXITPL=.FALSE.,EPW=0.05,
 &END
 &BLM
  IHFLAG=0,NTQW=19,
  TQW=1260.0,1260.0,1260.0,2770.0,3330.0,3960.0,4050.0,
    1156.32,1117.60,985.76,682.10,637.87,603.26,
    581.66,579.76,559.11,557.71,542.84,542.02,
  XTQW=  -13.0,-6.0,-2.26,-2.14,-1.57,-0.89,0.0,
     1.8722,3.06,4.406,8.4344,13.9624,
    23.6164,32.6124,40.3644,50.2504,62.4584,77.9624,95.7704,
  APROF=30.,200.,400.0,1009.0,NPROF=4,KDTPLT=1,NTR=800,
   KMTPLT=1,KTWPLT=1,XSEG=-14.0,10.0,33.0,56.0,79.0,101.23,NSEGS=5,
   XINO(1)=-14.0,-12.0,-10.0,-8.0,-6.0,-4.0,
   RINO(1)=2.054,2.054,2.054,2.054,2.054,2.054,
   UEO(1)=80.0,213.0,346.0,480.0,613.0,746.0,
   TEO(1)=6124.7,6123.8,6122.0,6120.2,6119.0,6118.0,
   PEO(1)=355.3,355.0,354.3,353.65,352.9,352.0,
 &END
```

Input for Reading 120

```
LOW T CPHS
H                    2
100.       4.968                              1
200.       4.968                              2
H2                   2
100.       6.729                              1
200.       6.560                              2
H2O                  2
100.       7.961                              1
200.       7.969                              2
O                    2
100.       5.665                              1
200.       5.433                              2
OH                   2
100.       7.798                              1
200.       7.356                              2
O2                   2
100.       6.956                              1
200.       6.961                              2
END LOW T CPHS
TITLE  HIGH E NOZZLE STUDY: E=1000 AND READING = 120
DATA
 &DATA
  ODE=1,ODK=1,TDK=0,BLM=0,IRPEAT=0,IOFF=6,
   RSI=0.5,ASUB=3.,1.5,NASUB=2,IRSTRT=0,
   ASUP=1.5,2.0,30.0,200.0,400.0,600.0,1024.0,NASUP=7,
   ECRAT=4.223,RI=2.,THETAI=25.,RWTU=2.,
   ITYPE=0,IWALL=4,RWTD=0.4,THETA=39.41,
   THE=7.94,NWS=36,
  RS=    0.0000,     1.1316,    1.1780,    1.2748,
       1.3704,    1.4198,    1.7658,    2.0876,
```

```
    2.4916,    3.0372,    5.2522,       5.7028,
       6.5606,    7.0420,    7.5072,    8.0464,
    9.0636,    9.5394,     10.6852,  12.0244,
   12.7284,     14.0056,  15.2408,  15.9610,
   16.6554,  17.3210,  18.7560,  19.6768,  20.5562,
   21.6918,  23.7554,  24.6744,   27.0428,
   29.1286,  30.1862, 32.0156,
  ZS=   0.0000,     0.3094,    0.3654,    0.4778,
        0.5908,    0.6480,    1.0430,    1.4050,
    1.8722,    2.5246,    5.5320,       6.2150,
       7.5802,    8.3862,    9.1920,  10.1592,
   12.0810,  13.0230,     15.4056,  18.4006,
   20.0684,     23.2606,  26.5588,  28.5824,
   30.6060,  32.6136,  37.1806,  40.2916,  43.4026,
   47.6334,  55.9914,  60.0166,  71.3698,
   82.7063,  89.0425,  101.2383,
 &END
REACTANTS
H 2.                                    00        100.              G294.40  F
O 2.                                    00        100.              G287.50  O

NAMELISTS
 &ODE
  RET=T,P=355.2,PSIA=T,OF=T,OFSKED=4.30,
   SUPAR=30.0,200.0,400.0,600.0,1024.0,ECRAT=4.223,
 &END
REACTIONS
  H + OH = H2O        , A=8.4E21 , N=2.0   , B=0.,  (AR) BAULCH 72 (A) 10U
  O + H  = OH         , A=3.62E18 , N=1.    , B=0.,  (AR) JENSEN 78 (B) 30U
  O + O  = O2         , A=1.9E13 , N=0.    , B=-1.79,  (AR) BAULCH 76 (A) 10U
  H + H  = H2         , A=6.4E17 , N=1.    , B=0.,  (AR) BAULCH 72 (A) 30U
END TBR REAX
  H2 + OH = H2O + H , A=2.20E13,  N=0.00,  B=5.15,  BAULCH 72 (A) 2U
  OH + OH =  H2O + O , A=6.30E12,  N=0.00,  B= 1.09,  BAULCH 72 (A) 3U
  H2 + O = H + OH   , A=1.80E10, N=-1.   , B=8.9,   BAULCH 72 (A) 1.5U
  O2 + H = O + OH   , A=2.2E14 , N=0.    , B=16.8,  BAULCH 72 (A) 1.5U
LAST REAX
THIRD BODY REAX RATE RATIOS
SPECIES H2,5.,5.,5.,4.,
SPECIES H2O,17.,5.,5.,10.,
SPECIES O2,6.,5.,11.,1.5,
SPECIES H,12.5,12.5,12.5,25.,
SPECIES O,12.5,12.5,12.5,25.,
SPECIES OH,12.5,12.5,12.5,25.,
LAST CARD
 &ODK
  EP=10.0,JPRNT=-2,MAVISP=1,XM(1)=1.0,NJPRNT=7,
   HI=0.01,HMIN=0.01,HMAX=0.01,
 &END
 &TRANS
  MP=200,
 &END
 &MOC
  EXITPL=.FALSE.,EPW=0.05,
 &END
 &BLM
  IHFLAG=0,NTQW=19,
  TQW=1260.0,1260.0,1260.0,2770.0,3330.0,3960.0,4050.0,
    1149.34,958.00,863.83,635.66,548.76,577.38,
    565.98,559.23,551.66,550.73,543.98,538.47,
  XTQW=   -13.0,-6.0,-2.26,-2.14,-1.57,-0.89,0.0,
     1.8722,3.06,4.406,8.4344,13.9624,
    23.6164,32.6124,40.3644,50.2504,62.4584,77.9624,95.7704,
  APROF=30.,200.,400.0,1009.0,NPROF=4,KDTPLT=1, NTR=800,
   KMTPLT=1,KTWPLT=1,XSEG=-14.0,10.0,33.0,56.0,79.0,101.23,NSEGS=5,
   XINO(1)=-14.0,-12.0,-10.0,-8.0,-6.0,-4.0,
   RINO(1)=2.054,2.054,2.054,2.054,2.054,2.054,
   UEO(1)=80.0,213.0,346.0,480.0,613.0,746.0,
   TEO(1)=5709.6,5709.0,5707.5,5706.0,5704.0,5702.2,
   PEO(1)=355.2,355.0,354.3,353.65,352.9,352.0,
 &END
```

Input for Reading 121

```
LOW T CPHS
H                    2
100.       4.968                                  1
200.       4.968                                  2
H2                   2
100.       6.729                                  1
200.       6.560                                  2
H2O                  2
100.       7.961                                  1
200.       7.969                                  2
O                    2
100.       5.665                                  1
200.       5.433                                  2
OH                   2
100.       7.798                                  1
200.       7.356                                  2
O2                   2
100.       6.956                                  1
200.       6.961                                  2
END LOW T CPHS
TITLE  HIGH E NOZZLE STUDY: E=1000 AND READING = 121
DATA
 &DATA
  ODE=1,ODK=1,TDK=1,BLM=1,IRPEAT=2,IOFF=6,
   RSI=0.5,ASUB=3.,1.5,NASUB=2,IRSTRT=0,
   ASUP=1.5,2.0,30.0,200.0,400.0,600.0,1024.0,NASUP=7,
   ECRAT=4.223,RI=2.,THETAI=25.,RWTU=2.,
   ITYPE=0,IWALL=4,RWTD=0.4,THETA=39.41,
   THE=7.94,NWS=36,
  RS=   0.0000,    1.1316,   1.1780,   1.2748,
        1.3704,   1.4198,   1.7658,   2.0876,
     2.4916,   3.0372,   5.2522,      5.7028,
        6.5606,   7.0420,   7.5072,   8.0464,
     9.0636,   9.5394,    10.6852,  12.0244,
    12.7284,    14.0056,  15.2408,  15.9610,
    16.6554,  17.3210,  18.7560,  19.6768,  20.5562,
    21.6918,  23.7554,  24.6744,   27.0428,
    29.1286,  30.1862, 32.0156,
  ZS=  0.0000,    0.3094,   0.3654,   0.4778,
        0.5908,   0.6480,   1.0430,   1.4050,
     1.8722,   2.5246,   5.5320,      6.2150,
        7.5802,   8.3862,   9.1920,  10.1592,
    12.0810,  13.0230,    15.4056,  18.4006,
    20.0684,    23.2606,  26.5588,  28.5824,
    30.6060,  32.6136,  37.1806,  40.2916,  43.4026,
    47.6334,  55.9914,  60.0166,  71.3698,
    82.7063,  89.0425,  101.2383,
 &END
REACTANTS
H 2.                                  00        100.              G295.00  F
O 2.                                  00        100.              G288.30  O

NAMELISTS
 &ODE
  RKT=T,P=360.0,PSIA=T,OF=T,OFSKED=5.11,
   SUPAR=30.0,200.0,400.0,600.0,1024.0,ECRAT=4.223,
 &END
REACTIONS
  H + OH = H2O        , A=8.4E21 , N=2.0   , B=0.,  (AR) BAULCH 72 (A) 10U
  O + H  = OH         , A=3.62E18 , N=1.    , B=0.,  (AR) JENSEN 78 (B) 30U
  O + O  = O2         , A=1.9E13 , N=0.    , B=-1.79,  (AR) BAULCH 76 (A) 10U
  H + H  = H2         , A=6.4E17 , N=1.    , B=0.,  (AR) BAULCH 72 (A) 30U
END TBR REAX
  H2 + OH = H2O + H , A=2.20E13,  N=0.00,  B=5.15,  BAULCH 72 (A) 2U
  OH + OH =  H2O + O , A=6.30E12,  N=0.00,  B= 1.09,  BAULCH 72 (A) 3U
  H2 + O = H + OH   , A=1.80E10, N=-1.  , B=8.9,   BAULCH 72 (A) 1.5U
  O2 + H = O + OH   , A=2.2E14 , N=0.   , B=16.8,  BAULCH 72 (A) 1.5U
LAST REAX
THIRD BODY REAX RATE RATIOS
SPECIES H2,5.,5.,5.,4.,
SPECIES H2O,17.,5.,5.,10.,
SPECIES O2,6.,5.,11.,1.5,
```

```
SPECIES H,12.5,12.5,12.5,25.,
SPECIES O,12.5,12.5,12.5,25.,
SPECIES OH,12.5,12.5,12.5,25.,
LAST CARD
 &ODK
  EP=0.0,JPRNT=-2,MAVISP=1,XM(1)=1.0,NJPRNT=7,
   HI=0.01,HMIN=0.01,HMAX=0.01,
 &END
 &TRANS
  MP=200,
 &END
 &MOC
  EXITPL=.FALSE.,EPW=0.05,
 &END
 &BLM
  IHFLAG=0,NTQW=19,
  TQW=1260.0,1260.0,1260.0,2770.0,3330.0,3960.0,4050.0,
     1057.56,922.32,873.83,641.26,598.97,572.43,
     563.59,558.51,552.33,545.82,542.90,537.82,
  XTQW=  -13.0,-6.0,-2.26,-2.14,-1.57,-0.89,0.0,
      1.8722,3.06,4.406,8.4344,13.9624,
     23.6164,32.6124,40.3644,50.2504,62.4584,77.9624,95.7704,
  APROF=30.,200.,400.0,1009.0,NPROF=4,KDTPLT=1,
   KNTPLT=1,KTWPLT=1,XSEG=-14.0,10.0,33.0,56.0,79.0,101.23,NSEGS=5,
   XINO(1)=-14.0,-12.0,-10.0,-8.0,-6.0,-4.0,
   RINO(1)=2.054,2.054,2.054,2.054,2.054,2.054,
   UEO(1)=81.0,216.0,351.0,486.0,621.0,757.0,
   TEO(1)=5614.0,5612.6,5610.4,5608.2,5607.0,5605.8,
   PEO(1)=360.0,359.6,358.3,357.65,356.0,355.9,
  NTR=800,
 &END
/EOF
```

Appendix D
Heat Rate-Uncertainty Analysis

The accuracy of the procedure used in obtaining values for heat rate was examined by using TDK. Heat-flux values which are predicted by the TDK program at axial locations corresponding approximately to experimental locations were examined. A curve of best fit of the heat-flux term ($q'' \pi 2R_i/\cos\theta$) as function of axial length) was drawn. This is equivalent to the experimental procedure. Integration yielded a heat rate of 117.61 kW (111.55 Btu/sec). This compares with the TDK prediction of 120.16 kW (113.98 Btu/sec). The integration procedure is accurate to within approximately 2 percent. It is important to realize that this does not mean that analytical and experimental values agree to that degree of accuracy.

References

1. Nickerson, G.R.; Dang, L.D.; and Coats, D.E.: Engineering and Programming Manual: Two-Dimensional Kinetic Reference Computer Program (TDK). (SN-63, Software and Engineering Associates; NASA Contract NAS8-35931) NASA-CR-178628, 1985.
2. Nickerson, G.R.: The Rao Method Optimum Nozzle Contour Program. Software and Engineering Associates Inc., Carson City, NV, SEA Report No. 6/82/800.1, June 1982.
3. Bittker, D.A.; and Scullin, V.J.: General Chemical Kinetics Computer Program for Static and Flow Reactions, with Application to Combustion and Shock-Tube Kinetics. NASA TN D-6586, 1972.
4. Evans, R.M.: Boundary Layer Integral Matrix Procedure—User's Manual. (Aerotherm—UM-75-64, Aerotherm Acurex Corp.; NASA Contract NAS8-30930) NASA CR-144046, 1975.
5. Keller, H.B.; and Cebeci, T.: Accurate Numerical Methods for Boundary Layer Flows, Pt. 2, Two-Dimensional Turbulent Flows. AIAA J., vol. 10, no. 9, Sept. 1972, pp. 1193-1199.
6. Cebeci, T.; and Smith, A.M.O.: Analysis of Turbulent Boundary Layers, Academic Press, 1974.
7. Smith, T.A.; Pavli, A.J.; and Kacynski, K.J.: A Comparison of Theoretical and Experimental Thrust Performance of a 1030:1 Area Ratio Rocket Nozzle at a Chamber Pressure of 2413 (350 kN/m^2 psia). NASA TP-2725, 1987.
8. Pavli, A.J.; Kacynski, K.J.; and Smith, T.A.: Experimental Thrust Performance of a High Area Ratio Rocket Nozzle. NASA TP-2720, 1987.
9. Back, L.H.; Cuffel, R.F.; and Massier, P.F.: Laminarization of a Turbulent Boundary Layer in Nozzle Flow—Boundary Layer and Heat Transfer Measurements with Wall Cooling. J. Heat Trans., vol. 92, no. 3, Aug. 1970, pp. 333-344.
10. Boldman, D.R.; Schmidt, J.F.; and Gallagher, A.K.: Laminarization of a Turbulent Boundary Layer as Observed from Heat-Transfer and Boundary-Layer Measurements in Conical Nozzles. NASA TN D-4788, 1968.
11. Praharaj, S.C.: Boundary Layer Simulator (BLIMPJ) Improvement. The 22nd JANNAF Combustion Meeting, Vol. 1, CPIA-PUBL-432, Chemical Propulsion Information Agency, 1985, pp. 477-493. (Avail. NTIS, AD-A165503).

NASA
National Aeronautics and Space Administration

Report Documentation Page

1. Report No.	2. Government Accession No.	3. Recipient's Catalog No.
NASA TP-2726		

4. Title and Subtitle	5. Report Date
Experimental Evaluation of Heat Transfer on a 1030:1 Area Ratio Rocket Nozzle	August 1987
	6. Performing Organization Code: 506-42-21

7. Author(s)	8. Performing Organization Report No.
Kenneth J. Kacynski, Albert J. Pavli, and Tamara A. Smith	E-3558
	10. Work Unit No.

9. Performing Organization Name and Address	11. Contract or Grant No.
National Aeronautics and Space Administration Lewis Research Center Cleveland, Ohio 44135	13. Type of Report and Period Covered: Technical Paper

12. Sponsoring Agency Name and Address	14. Sponsoring Agency Code
National Aeronautics and Space Administration Washington, D.C. 20546	

15. Supplementary Notes

Prepared for the 23rd Joint Propulsion Conference cosponsored by the AIAA, SAE, ASME, and ASEE, San Diego, California, June 29—July 2, 1987. AIAA report number, AIAA-87-2070.

16. Abstract

Accurate determination of heat flux in the divergent portion of high-area-ratio rocket nozzles is important not only in designing the nozzles but also in predicting their performance. Although much work has been done in obtaining experimental heat-flux values in the chamber and throat sections of rocket engines, little data has been taken in the divergent portion, especially for high-area-ratio nozzles (200:1 to 1000:1). At the NASA Lewis Research Center's Rocket Engine Test Facility, a 1030:1 carbon steel, heat-sink nozzle was tested. The test conditions included a nominal chamber pressure of 2413 kN/m^2 (350 psia) and a mixture ratio range of 2.78 to 5.49. The propellants used were gaseous oxygen and gaseous hydrogen. The nozzle had thermocouples placed on the outer wall at various axial locations. The outer-wall temperature measurements were used to calculate the inner-wall temperature and the heat flux and heat rate to the nozzle at specified axial locations. The experimental heat fluxes were compared to those predicted by the December 1984 version of the Two-Dimensional Kinetics (TDK) computer analysis program. When laminar boundary-layer flow was assumed in the analysis, the predicted values were within 15 percent of the experimental values for area ratios of 20 to 975. However, when turbulent-boundary layer conditions were assumed, the predicted values were approximately 120 percent higher than the experimental values. A study was performed to determine if the conditions within the nozzle could sustain a laminar boundary layer. Using the flow properties predicted by TDK, we calculated the momentum-thickness Reynolds number and predicted the point of transition to turbulent flow. The predicted transition point was within 0.5 in. the nozzle throat. Calculations of the acceleration parameter were then made to determine if the flow conditions could produce relaminarization of the boundary layer. It was determined that if the boundary-layer flow was inclined to transition to turbulent, the acceleration conditions within the nozzle would tend to suppress turbulence and keep the flow laminarlike.

17. Key Words (Suggested by Author(s))	18. Distribution Statement
Heat flux Rocket nozzle Nozzle design High-area-ratio rocket nozzle	Unclassified—unlimited STAR Category 20

19. Security Classif. (of this report)	20. Security Classif. (of this page)	21. No of pages	22. Price*
Unclassified	Unclassified	26	A03

*For sale by the National Technical Information Service, Springfield, Virginia 22161